ProteasomeID: quantitative mapping of proteasome interactomes and substrates for in vitro and in vivo studies

Aleksandar Bartolome[1], Julia C. Heiby[1*], Therese Dau[1*], Domenico Di Fraia[1], Ivonne Heinze[1], Joanna M. Kirkpatrick[1] and Alessandro Ori[1,#]

Affiliations:

1 - Leibniz Institute on Aging - Fritz Lipmann Institute (FLI), Jena, Germany

* equal contribution

correspondence to: alessandro.ori@leibniz-fli.de

SUMMARY

Proteasomes are essential molecular machines responsible for the degradation of proteins in eukaryotic cells. Altered proteasome activity has been linked to neurodegeneration, auto-immune disorders and cancer. Proteasomes have been exploited for the development of small molecule degraders for otherwise undruggable proteins. Despite the relevance for human disease and drug development, no method currently exists to monitor proteasome interactions *in vivo* in animal models. To fill this gap, we developed a strategy based on tagging of proteasomes with promiscuous biotin ligases and generated a new mouse model enabling the quantification of proteasome interactions by mass spectrometry. We show that biotin ligases can be incorporated in fully assembled proteasomes without negative impact on their activity. We demonstrate the utility of our method by identifying novel proteasome-interacting proteins, charting interactomes across mouse organs, and showing that proximity-labeling enables the identification of both endogenous and small molecule-induced proteasome substrates.

Keywords: proteasome, BioID, mass spectrometry, protein degradation, proximity labeling, mouse model

INTRODUCTION

The ubiquitin–proteasome system (UPS) is a major selective protein degradation system of eukaryotic cells [1]. Proteasomes influence crucial processes in the cell including protein homeostasis, DNA repair, signal transduction and immune responses [2] by degrading a multitude of regulatory, short-lived, damaged and misfolded proteins [3 4]. Impairment of proteasome function has been described to occur during aging [5] and in neurodegenerative diseases [6 1], and the expression levels of proteasome subunits has been linked to longevity in different species including worms [7], fish [8] and flies[9 10]. Partial proteasome inhibition is sufficient to induce cellular senescence [11 12] and this cytostatic property has been exploited in cancer therapies, e.g., against blood cancers [13]. Furthermore, the role of proteasomes extends beyond the degradation of proteins. In the immune system, peptide generation by specialized immunoproteasomes regulates antigen presentation and has been linked to auto-immune disorders [14].

In recent years, drug development efforts have focused on hijacking the UPS for the development of selective degraders of otherwise undruggable proteins [15]. Protein degraders, such as proteolysis targeting chimera (PROTAC), are typically composed of 3 key elements: (i) an E3 ubiquitin ligase ligand, (ii) a ligand that binds the target protein, and (iii) a linker binding the two ligands. PROTACs bring the E3 ubiquitin ligase in proximity to the protein of interest, resulting in target protein ubiquitination and degradation by cellular proteasomes. So far, protein degraders have been developed for more than 50 targets including protein kinases, nuclear receptors, and transcriptional regulators [16]. However, bottlenecks have emerged in the development of protein degraders. For instance, induction of proximity between the target protein and the E3 ligase does not always result in protein ubiquitination, and, additionally, in some cases protein ubiquitination does not induce protein degradation [17]. Therefore, analytical approaches that enable monitoring whether candidate compounds can bring the target protein into direct contact with cellular proteasomes could drastically speed up the development of new protein degraders.

The composition of cellular proteasomes can be heterogeneous due to the assembly of distinct sub-complexes in variable stoichiometries, and to the incorporation of tissue/cell type specific components. Specialized proteasomes have been described in immune cells, thymus, and sperm cells [18]. At the subcellular level, proteasomes constantly shuttle between the cytoplasm and nucleus [19], interact with inner nuclear membrane [20], endoplasmic reticulum [21], Golgi [22] and plasma

membranes [23]. Therefore, there is a strong need for methods capable of detecting proteasome interactions and substrates *in situ* across different cellular compartments and with cell-type resolution.

Here, we present an approach named ProteasomeID that enables the quantification of proteasome interacting proteins and substrates in cultured human cells and mouse models. The approach entails tagging the proteasome with promiscuous biotin ligases, which are incorporated into fully assembled proteasomes without affecting their activity. The ligases label with biotin proteins that come into proximity (~10 nm) of the tagged proteasome subunit. Biotinylated proteins are then captured from cell or tissue lysates using an optimized streptavidin enrichment protocol and analyzed by deep Data Independent Acquisition (DIA) mass spectrometry. We show that ProteasomeID can quantitatively monitor the majority of proteasome interacting proteins both in cultured cells and *in vivo* in mice, and identify novel proteasome interacting proteins. In addition, when combined with proteasome inhibition (e.g., by MG132), ProteasomeID enables the identification of known endogenous proteasome substrates, including low abundant transcription factors that are typically challenging to quantify by mass spectrometry-based proteomics. Finally, ProteasomeID can be used to directly monitor the ability of small molecule degraders to induce the recruitment of target proteins to proteasomes within cells.

RESULTS

Design of a proximity labeling strategy to monitor proteasome interactions

Since the proteasome consists of two distinct sub-complexes (20S core and 19S regulatory particle), we generated two cell lines that enabled monitoring the interactions of each sub-complex separately. We fused the promiscuous biotin ligase BirA* at the C-termini of the core particle protein PSMA4 and the regulatory particle protein PSMC2 (Figure 1A). Each construct also contained a FLAG tag for fusion protein detection. We used these constructs to generate stable HEK293 FlpIn TREx (HEK293T) cell lines that overexpress the BirA* fusion proteins under the control of a tetracycline inducible promoter. A cell line expressing only the BirA* protein was used as control to account for nonspecific biotinylation. We confirmed tetracycline-dependent expression of PSMA4-BirA* and PSMC2-BirA* in the corresponding cell lines by anti-FLAG immunoblot and confirmed biotinylating activity following supplementation of exogenous biotin using streptavidin-HRP blot (Figure 1B). Results were validated by immunofluorescence analysis

(Figure 1C and S1A). Since the BirA* fusion proteins are over-expressed using a CMV promoter, we also confirmed that the abundance levels of PSMA4-BirA* are comparable to the ones of the endogenous PSMA4 using an anti-PSMA4 immunoblot (Figure 1D). To assess the influence of BirA* fusion proteins on proteasome function, we measured proteasome chymotrypsin-like activity in cell lysates from BirA* expressing cell lines in presence or absence of tetracycline. We observed a slight reduction of proteasome activity (~15-20%) following addition of tetracycline that was comparable between cell lines expressing proteasome BirA* fusion proteins and BirA* control (Figure 1E). We therefore concluded that the slight reduction in proteasome activity observed likely results from the overexpression of the construct proteins rather than from the interference with the normal proteasome function by the fusion of BirA* to proteasome subunits. To confirm the correct assembly of BirA* fusion proteins into proteasome complexes, we performed Size Exclusion Chromatography coupled to quantitative mass spectrometry (SEC-MS) analysis of the cell line expressing PSMA4-BirA* following induction by tetracycline. Protein elution profiles built from mass spectrometry data using the estimated abundance of proteins in each fraction revealed three major distinct peaks corresponding to the major assembly states of the proteasome. These include 30S proteasomes, containing a core particle capped with 2 regulatory particles, 26S proteasomes, containing a core particle capped with 1 regulatory particle, and isolated core particles (20S proteasomes) (Figure 1F). Except for a peak in lower molecular weight fractions, likely representing intermediate complex assemblies, most of the BirA* signal correlated with the elution profile of other proteasome components in all the assembly states, indicating correct incorporation of the PSMA4-BirA* fusion protein in assembled proteasome complexes (Figure 1F).

ProteasomeID retrieves proteasome subunits and known proteasome interactors

In order to identify biotinylated proteins by tagged proteasomes, we optimized a BioID protocol that we previously developed [24]. Briefly, the protocol entails capture of biotinylated proteins from cell lysates using streptavidin beads followed by enzymatic on bead digestion and analysis of digested peptides by liquid chromatography tandem mass spectrometry (LC-MS/MS). We introduced chemical modification of streptavidin beads and changed the protease digestion strategy to reduce streptavidin contamination following on bead digestion (Figure S2A). In addition, we implemented Data Independent Acquisition (DIA) for the analysis of the resulting peptides by mass spectrometry. These optimizations allowed us to drastically reduce (>4 fold) the background from streptavidin-derived peptides (Figure S2B, Figure S2C), and to increase more

than 2-fold the number of identified proteins and biotinylated peptides in our BioID experiments (Figure S2D).

Using this optimized BioID protocol, we analyzed samples enriched from four biological replicates of cell lines expressing PSMA4-BirA*, PSMC2-BirA* or BirA* control. Principal component analysis (PCA) showed clear separation between the 3 experimental groups (Figure 2A). Volcano plots highlighted proteasome subunits and known interactors showing strong levels of enrichment (typically >4 fold) compared to BirA*-expressing control cell line (Figure 2B and Table S1). By overlaying our data on the known proteasome structure (Chen et al. 2016), we could show near to complete coverage of proteasome components and, expectedly, differential levels of enrichment for the 19S or 20S particle depending on the tagged proteasome member (Figure 2C). We also demonstrated the specificity of protein biotinylation by confirming that 25 out of 26 residues identified as biotinylated by PSMA4-BirA* indeed are less than 10 nm away from the bait protein on the proteasome structure (Figure 2D).

Next, we investigated the retrieval of known interacting proteins using the following two approaches. First, we compared the BioID data from PSMA4-BirA* to the SEC-MS data obtained from the same cell line. We could show that proteins significantly enriched in BioID display higher correlation of SEC-MS elution profiles with the bait protein PSMA4 than not-enriched proteins (Figure 2E). Second, we compared the proteins identified as enriched either in PSMA4-BirA* or PSMC2-BirA* to an independent study based on protein correlation profiling performed in different cell types [25]. This analysis showed that our experiments could retrieve 70% (51 out 73) of the proteasome interacting proteins identified in this previous study, but also several potential novel candidate interaction partners (Figure 2F).

Synaptojanin 1 and other phospho-inositol phosphatases interact with the proteasome

Beyond known proteasome interacting partners and proteins involved in ubiquitin cycle, ProteasomeID highlighted two groups of proteins that were underrepresented in previous studies: proteins involved in vesicular trafficking and phospholipid metabolism (Figure 3A, 3B and Table S1). Hits belonging to both groups were present in the top 125 interactors of both core and regulatory particles. Among these proteins, SYNJ1 (also known as PARK20) is a phospho-inositol phosphatase with a regulatory role in clathrin-mediated endocytosis [26] [27] [28] [29] that was not previously described as a proteasome interactor. We detected this protein as significantly enriched in ProteasomeID from both PSMA4-BirA* and PSMC2-BirA* cell lines (Figure 3C). In addition, SEC-MS data showed significant co-elution between PSMA4 and SYNJ1 (Figure 3D),

independently supporting a potential interaction between assembled proteasomes and SYNJ1. Closer examination of the ProteasomeID dataset revealed other phospho-inositol phosphatases to be enriched in both PSMA4-BirA* and PSMC2-BirA* BioID samples, suggesting a broader interaction of the proteasome with this class of enzymes (Figure 3E).

To validate this potential novel interaction, we used two independent strategies. First, we designed a reciprocal BioID experiment by tagging SYNJ1 with BirA* either N- or C-terminally. We verified expression of the fusion proteins with anti-FLAG immunoblot (Figure S3A) and biotinylation efficiency using Streptavidin-HRP on lysates from the generated cell lines (Figure S3B), and confirmed the results using immunofluorescence (Figure S3C, S3D). Next, we applied the optimized BioID protocol to cell lines expressing SYNJ1 fused to BirA* and compared them to the BirA* control line. We could retrieve known SYNJ1 interacting proteins, e.g., SNX9, SH3GL1, SH3GL2, SH3KBP1, and other proteins involved in vesicular trafficking, e.g., CD2AP, GOLGA4, ITSN2, SH3GLB2 (Figure 4A and Table S2). Among the proteins significantly enriched in both SYNJ1-BirA* and BirA*-SYNJ1 BioID experiments relatively to BirA* control line, we identified a subset of proteasome subunits from both 20S and 19S particles (Figure 4B). Consistently, direct comparison of proteasome and SYNJ1 interactomes revealed a shared network of interacting proteins involved in membrane trafficking (Figure 4C).

As a second independent approach, we attempted to verify the SYNJ1-proteasome interaction using immunoprecipitation. However, we were unable to detect SYNJ1 in proteasome immunoprecipitates, suggesting that this type of interactions might be disrupted following cell lysis. Therefore, we instead used proximity ligation assay (PLA) [30] using antibodies against the 20S proteasome α-subunits 1-7 and SYNJ1. We performed PLA in HEK293T cells expressing PSMA4-BirA* as well as wild type U2OS cells. The latter was included to test interaction between endogenous proteasomes and SYNJ1. We could detect PLA signal in both PSMA4-BirA* expressing cells as well as wild type U2OS cells, while the respective negative controls showed minimal or absent background signal (Figure 4D). These results confirmed *in situ* proximity between SYNJ1 and the proteasome.

A mouse model for *in vivo* ProteasomeID

Having established and validated proximity labeling of proteasomes in a cell culture model, we designed a strategy to implement ProteasomeID in a mouse model (Figure 5A). The mouse model was designed to express the 20S proteasome core particle PSMA4 fused to the biotinylating enzyme miniTurbo and a FLAG tag for the detection of the fusion protein. We chose miniTurbo

instead of BirA* because of its higher biotinylating efficiency [31]. PSMA4-miniTurbo was inserted in the Col1a1 locus downstream of a tetracycline responsive element (TRE) in the D34 mouse embryonic stem cell line [32]. This line carries a cassette encoding the rTA3 transactivator and the fluorescent protein mKate on the Rosa 26 locus under the control of a CAG promoter. Importantly, a lox-stop-lox cassette is present between the CAG promoter and the rTA3 and mKate expressing cassette, enabling tissue-specific expression via crossing to specific CRE lines. The engineered D34 line was used to generate a mouse line via blastocyst injection. For proof of concept, we crossed the TRE-Psma4-miniTurbo;Rosa26-CAGs-RIK line with a CMV-Cre line that expresses constitutively the CRE recombinase in all tissues [33]. After confirming successful excision of the lox-stop-lox cassette (Figure S4A), the obtained TRE-Psma4-miniTurbo;Rosa26-CAGs-RIK line was back crossed to C57BL6/J to remove the CMV-Cre allele. The obtained mouse line constitutively expresses the rTA3 transactivator, thereby enabling doxycycline inducible expression of PSMA4-miniTurbo in all tissues.

We assigned eight animals of the desired genotype to two experimental groups: treatment group and a control group (Figure 5B). The treatment group was fed doxycycline-containing food throughout the 14 days experiment to induce the expression of PSMA4-miniTurbo. The control group was fed regular chow. After a week of this regime, both groups were submitted to daily subcutaneous injections of biotin for a week. We chose 14 days of doxycycline induction prior to biotin injection based on the average half-life of proteasomes estimated *in vivo* [34]. We observed neither significant changes in body weights nor any sign of suffering in both experimental groups for the duration of the experiment (Figure 5C). Following treatment, animals were sacrificed and liver, brain, heart, skeletal muscle, and kidney were collected for further analysis.

We first analyzed total proteomes from the collected organs by DIA mass spectrometry. By comparing the relative abundance of peptides derived from miniTurbo, we confirmed successful induction of PSMA4-miniTurbo in all the organs following feeding with doxycycline-containing food (Figure 5D). The induction of PSMA4-miniTurbo did not alter the total levels of PSMA4 proteins, suggesting compensation of the endogenous protein, as observed in HEK293T cells (Figure 1D). However, the level of induction varied between organs. By comparing estimates of absolute protein abundance derived from the mass spectrometry data, we could estimate that in the kidney the levels of the tagged PSMA4-miniTurbo varied between 69.7% of the total PSMA4 and 8.2% in the heart (Figure 5D). We also confirmed successful increase of protein biotinylation by immunohistochemitry analysis of liver tissue following PSMA4-miniTurbo induction and biotin supplementation (Figure S4B).

Mass spectrometry analysis of biotinylated proteins revealed successful enrichment of proteasome components and known interacting proteins in all organs following feeding with doxycycline-containing food (Figure 5E and Table S3). However, the number of *bona-fide* proteasome-interacting proteins identified and their enrichment (log2 fold change) varied among organs, being most prominent in kidney and liver and especially low in the brain. This was in line with the different absolute levels of PSMA4-miniTurbo detected by whole organ proteome analysis (Figure 5D). We next compared the candidate proteasome-interacting proteins identified in HEK293T cells and mouse organs, and related them to previously reported interactors (Figure 5F). We were able to identify a significant overlap between the HEK293T and mouse interactomes and retrieved >50% of the previously reported proteasome-interacting proteins. In addition, we detected 136 potential novel candidate proteasome interacting proteins that were consistently identified both *in vitro* and *in vivo* (Table S4), including the phospho-inositol phosphatase INPP5B and the adapter protein ITSN2, which were also found to be shared interactors between proteasomes and SYNJ1 in cultured cells (Table S2). Together these data demonstrate that proteasome interacting proteins can be quantified from mouse organs using ProteasomeID.

Identification of proteasome substrates by ProteasomeID

Having demonstrated that ProteasomeID can be used both in cultured cells and *in vivo* to obtain snapshots of the proteasome interactome, we next investigated whether we could use this approach to directly identify proteasome substrates. We reasoned that under steady state conditions the interaction between proteasomes and their substrates might be too short lived to enable efficient biotinylation. Therefore, we generated HEK293T cells expressing PSMA4-miniTurbo enabling shorter biotinylation time (2h vs. 24h) thanks to the enhanced activity of miniTurbo as compared to BirA* [31] (Figure S5A, S5B). We confirmed enrichment of proteasome members and interacting proteins (Figure S5C) and observed positive correlation between the enrichments measured using PSMA4-miniTurbo and PSMA4-BirA*, relatively to their respective control lines (Figure S5D). Next, we included a step of acute inhibition of the proteasome by the potent cell-permeable inhibitor MG132 for 4h prior to biotin supplementation (Figure 6A). Principal component analysis revealed a clear impact of proteasome inhibition on the biotinylated proteins quantified by mass spectrometry (Figure 6B). Direct comparison of pull downs from cells treated with MG132 versus control cells revealed prominent enrichment of proteasome activators and ubiquitin (Figure 6C and Table S5), consistent with the recruitment of proteasome activators and direct ubiquitination of proteasome members following inhibition [35]. To identify potential proteasome substrates, we focused on a subset of 296 proteins that were enriched relative to

miniTurbo control only in presence of MG132 (Figure S5E and Table S5). Among these, we found well characterized proteasome substrates including the transcription factors ATF4, HIF1A, JUN and MYC, several proteins mediating ER stress response such as XBP1, as well as cell-cycle regulated proteins such as CDC7, CDT1 and CDKN2A (Figure 6D and S5E). Consistently, the majority of these proteins increased in their total abundance following MG132 treatment (Figure S5F) and more than half of them (154/296, 52%) showed increased ubiquitination following MG132 treatment in an independent study [36] (Table S5).

Finally, we investigated whether we could use the same strategy to identify selective induction of protein degradation by small molecules. For this purpose, we used KB02-JQ1, a well-characterized PROTAC that targets bromodomain-containing proteins (BRDs) for proteasomal degradation [37]. We treated cells with KB02-JQ1 for 8 hours prior to proteasome inhibition and biotin supplementation (Figure 6E). Mass spectrometry analysis showed no global changes induced by KB02-JQ1 in either presence or absence of MG132, as indicated by PCA (Figure 6F). However, we could detect prominent enrichment of BRD containing proteins following treatment with KB02-JQ1 (Figure S5G). The effect was more pronounced for BRD2 and BRD3 and less striking for BRD4 (Figure 6G), presumably reflecting different kinetics of induced degradation by KB02-JQ1 [37]. Notably, the enrichment of BRD2 and BRD3 was also detectable in absence of MG132, in contrast to endogenous substrates that become enriched only following proteasome inhibition (Figure 6D). Together, these data demonstrate that ProteasomeID can be used to detect both endogenous and protein degrader-induced substrates of the proteasome in cultured cells.

DISCUSSION

Our study demonstrates the versatility of proximity labeling for detecting proteasomal protein-protein interactions both *in vitro* and *in vivo*. Comparison to a Protein Correlation Profiling coupled to Mass Spectrometry (PCP-MS) approach previously used to probe for proteasome interactors in different cell types [25] showed that ProteasomeID can retrieve more than half of the known proteasome-interacting proteins in a single experiment. Interactors reported by PCP-MS but not detected by ProteasomeID were predominantly proteins not expressed in HEK293 cell lines, such as immunoproteasome subunits. Our data further expands the repertoire of proteasome interactors by being able of detecting both strong interactors like members of the COP signalosome complex, as well as transient protein-protein interactions exemplified by USP14 - a reversibly associating subunit of the 19S particle [38]. We revealed novel molecular interactions between proteasomes and a set of phosphatidylinositol phosphatases that might underlie a

previously unappreciated role for the proteasome in vesicular trafficking and phospholipid metabolism via, e.g., Synaptojanin 1 (SYNJ1). Importantly, we were unable to detect this type of interactions using immunoprecipitation approaches. This indicates that proximity labeling might be particularly suited for identifying interactions between proteasomes and membrane-associated proteins that might have been missed by traditional approaches that require cell lysis. Further studies will be required to elucidate the functional role of the interactions between proteasome and phosphatidylinositol phosphatases.

We demonstrated that ProteasomeID can be successfully implemented in living animals allowing us to quantify proteasome interacting proteins in multiple mouse tissues. The expression of tagged proteasomes did not negatively impact animal well-being in both sexes. However, we noted that the relative levels of tagged proteasomes varied between organs, limiting the efficiency of ProteasomeID, e.g., in heart and brain. The locus used for PSMA4-miniTurbo expression (Col1a1) is known to be active in all the organs tested [39] and doxycycline is broadly bioavailable and can pass the brain-blood barrier [40]. Therefore, we speculate that the different levels of proteasome tagging observed might be due to differences in protein turnover among organs [41] that could limit the incorporation of tagged subunits in newly assembled proteasomes. In such a scenario, longer doxycycline induction periods might enable higher levels of biotin ligase incorporation into proteasomes also in challenging organs such as heart and brain. In the future, crossing the ProteasomeID mouse with lines expressing the Cre recombinase under the control of specific drivers will enable the study of proteasome composition and interactions with cell type resolution *in vivo*. In addition, the ProteasomeID mouse opens new opportunities for future mechanistic studies on the involvement of proteasomes in neurodegenerative, malignant, inflammatory, and metabolic diseases by means of crossing with established disease models.

The combination of proximity labeling and proteasome inhibition enabled the identification of known proteasome activators and endogenous substrates of the proteasome, including low abundant proteins such as transcription factors that are typically challenging to quantify by bulk proteomic analysis. This strategy could be used in the future to monitor how perturbation of cellular proteostasis by different proteotoxic stress, e.g., protein aggregate formation [42], influences the protein degradation landscape of the proteasome, or to monitor dynamic changes in proteasome interactions and substrates, e.g., during the cell cycle, cell differentiation or cancer transformation.

Finally, we showed that ProteasomeID can directly identify known targets of PROTACs within cells. It is conceivable that the same strategy can be adapted to mouse models using the ProteasomeID mouse that we developed. This would enable assessing the efficacy of protein degraders in specific organs or cell types *in vivo.* In the future, quantification of the proteasome-associated proteome by ProteasomeID could greatly complement other existing approaches such as mass spectrometry analysis of proteolytic peptides (MAPP) [43] to profile the proteasome degradation landscape in physiological and disease models, and to comprehensively assess the efficacy and specificity of protein degraders.

Acknowledgments. The authors gratefully acknowledge support from the FLI Core Facilities Proteomics, Imaging, Functional Genomics, Histology & Electron Microscopy and the Mouse Facility. The authors acknowledge Anja Baar, Christoph Kaether, and Ellen Spät for support with animal experiments. AO acknowledges funding from the DFG (RTG2155 ProMoAge), the Else Kröner Fresenius Stiftung (award number: 2019_A79), the Deutsches Zentrum für Herz-Kreislaufforschung (award number: 81X2800193), the Fritz-Thyssen foundation (award number: 10.20.1.022MN), and the Chan Zuckerberg Initiative Neurodegeneration Challenge Network (award numbers: 2020-221617 and 2021-230967). The FLI is a member of the Leibniz Association and is financially supported by the Federal Government of Germany and the State of Thuringia.

Author contributions. Conceptualization: AB, JH, TD, JMK, AO. Investigation: AB, IH, JMK. Methodology: AB, JMK. Data analysis: AB, DDF, AO. Project administration: AO. Resources: AO. Supervision: JH, TD, AO. Visualization: AB, DDF, AO. Writing – original draft: AB, AO. Writing – review & editing: JH, TD and JMK.

Declaration of interests. Authors A.B., J.H., T.D., J.M.K. and A.O. are inventors of patent application DE 10 2022 117 634.7 describing this method.

METHODS

Chemicals. The following chemicals were obtained from Sigma Aldrich: Dulbecco's modified Eagle's medium (DMEM) high glucose 4.5 g/l(Sigma Aldrich, D6429), L-Glutamine (Sigma Aldrich, G7513), biotin (Sigma Aldrich, B4501), PBS (Sigma Aldrich, D8537), cOmplete™ Mini EDTA-free Protease Inhibitor (Sigma, 04693132001), Tetracycline (Sigma Aldrich, 87128), HEPES (Sigma Aldrich, H3375), Sodium dodecyl sulfate (SDS) (Sigma Aldrich, 75746), PonceauS (Sigma Aldrich, P7170), Sodium deoxycholate from (Sigma Aldrich, 30970), Naphtol blue black (Sigma Aldrich, N3393), Adenosine triphosphate (ATP) (Sigma Aldrich, A2383), MG-132 (Sigma Aldrich, M7449), MG-132 (Sigma Aldrich, 474787), Duolink® Blocking Solution and Duolink® Antibody Diluent and Duolink® In Situ PLA® Probe Anti-Mouse MINUS (Sigma Aldrich, DUO92004), Duolink® In Situ wash buffer A and Duolink® In Situ Wash Buffer B (Sigma Aldrich, DUO82049), Duolink® In Situ PLA® Probe Anti-Rabbit PLUS (Sigma Aldrich, DUO92002), Ligase from Duolink® In Situ Detection Reagents Red kit and Polymerase from Duolink® In Situ Detection Reagents Red kit and 5x Amplification Red buffer from Duolink® In Situ Detection Reagents Red kit (Sigma Aldrich, DUO92008), Duolink® In Situ Mounting Medium with DAPI (Sigma Aldrich, DUO82040), NP-40 (Sigma Aldrich, I8896), KCl (Sigma Aldrich, P3911), Iodoacetamide (Sigma Aldrich, I1149), Dimethyl sulfoxide (Sigma Aldrich, D2438).

The following chemicals were obtained from Thermo Fisher Scientific: Hygromycin B (Thermo Fisher Scientific, 10687010), Trypsin-EDTA (Thermo Fisher Scientific, 25300-062), Zeocin™ (Thermo Fisher Scientific, R25001), Enhanced chemiluminescence detection kit (ECL) (Thermo Fisher Scientific, 32209), Sulfo-NHS-Acetate (Thermo Fisher Scientific, 20217), DAPI (4',6-Diamidino-2-Phenylindole, Dihydrochloride) (Thermo Fisher Scientific, D1306), Permafluor mounting medium (TA-006-FM, Thermo Fisher), Poly-D-Lysin (Thermo Fisher Scientific, A3890401).

The following chemicals were obtained from Carl Roth: D(+)-biotin (Carl Roth, 3822.1), EDTA (Carl Roth, 8043.2), EGTA (Carl Roth, 3054.1), NaCl (Carl Roth, 3957.1), Triton X-100 (Carl Roth, 3051.3), Tris (Carl Roth, 4855.2), Glycerin (Carl Roth, 7533.1), β-mercaptoethanol (Carl Roth, 4227.3), Tween-20 (Carl Roth, 9127.1), Bovine serum albumin (Carl Roth, 3737.3), Acetic acid (Carl Roth, 6755.1), Aprotinin (Carl Roth, A162.3), Leupeptin (Carl Roth, CN33.2), Ammonium bicarbonate (Carl Roth, T871.2), Formic acid (Carl Roth, 4724.3), Formaldehyde (Carl Roth, CP10.1).

The following chemicals were obtained from Biosolve: Methanol (Biosolve, 0013684102BS), Acetone (Biosolve, 0001037801BS), Formic acid (Biosolve, 0006914143B5), Trifluoracetic acid (Biosolve, 0020234131BS), Acetonitrile (Biosolve, 0001204102BS), 2-propanol (Biosolve, 0016264101BS).

The following chemicals were obtained from Roche: X-tremeGENE 9 DNA Transfection Reagent (Roche, 06365779001), Phosphatase inhibitors (Roche, 04906837001), protease inhibitors (Roche, 04693159001).

The following chemicals were obtained from Invitrogen: Goat serum (Invitrogen, 31872), Streptavidin Alexa Fluor™ 568 (Invitrogen, S11226), EZQ® Protein Quantitation Kit (Invitrogen, R33200).

The following chemicals were obtained from Gibco: Fetal bovine serum (FBS) (Gibco™, 10270-106) and Blasticidin (Gibco™, R21001).

The following chemicals were obtained from Merck: Streptavidin coated Sepharose beads (Merck, GE17-5113-01), $MgCl_2$ (Merck, 8.14733.0100).

Trypsin was obtained from Promega (Promega, V511 sequencing grade). LysC was obtained from Wako (Wako, 125-05061 sequencing grade). Phusion® High-Fidelity DNA Polymerase was obtained from New England Biolabs (New England Biolabs, M0530S). Glycine was obtained by VWR (VWR, 1042011000). Turbonuclease was obtained from MoBiTec (MoBiTec GmbH, GE-NUC10700-01). KB02-JQ1 was purchased from MedChemExpress (MedChemExpress, Cat. No. HY-129917). Urea was obtained from Bio Rad (Bio Rad, 161-0730). iRT peptides were obtained from Biognosys (iRT kit, Biognosys, Zurich, Switzerland). HPLC Column check standards were obtained from Phenomenex (Phenomenex, ALO-3042). 20S proteasome activity assay kit was obtained from Millipore (Millipore, APT280). Mice food was obtained from ssniff: standard chow (ssniff, V1524-786) or with doxycycline containing food (ssniff, A153D00624). From VWR following chemicals were obtained: xylene (VWR, 28973.363), ethanol (VWR, 85830.360).

Antibodies. Following antibodies were used: anti-FLAG® M2 (1:1000, Sigma Aldrich, F3165), Streptavidin HRP (1:40000, Abcam ab7403), anti-PSMA4 (1:250, NOVUS biologicals NBP2-38754), anti-SYNJ1 (1:250, Sigma Aldrich, HPA011916), anti-β-actin (1:5000, Sigma Aldrich, A5441), anti-rabbit HRP-conjugated (1:2000, Dako P0448), anti-mouse HRP-conjugated (1:1500, Dako P0447), anti-FLAG® (1:100, Sigma Aldrich, F7425), anti-mouse-Cyanine5 (1:400, Thermo Fisher Scientific, A10524), Streptavidin Alexa Fluor™ 568 (1:2000, Invitrogen, S11226), anti-Proteasome 20S alpha 1+2+3+5+6+7 (1:200, Abcam, ab22674).

Mice. Rosa26 mice (B6.Cg-Col1a1tm1(tetO-cDNA:Psma4)Mirim/J; B6.Cg-Gt(ROSA)26Sortm2 (CAG-rtTA3,-mKate2)Slowe/J) (Dow et al., 2014) were generated by Mirimus Inc. (NY, USA). All animals were housed (2-5 mice per cage) at the Leibniz Institute on Aging- Fritz Lipmann Institute, in environmentally controlled, pathogen-free animal facility with a 12 h light/ 12 h dark cycle and fed ad libitum with a standard chow or with the doxycycline containing food. Animals used for the procedure were 2-4 months old. Biotin (24mg/kg body weight) or PBS were administered subcutaneously, daily for 7 consecutive days. At the end of the regime, mice were euthanized with CO_2 in a CO_2 chamber (VetTech Solutions Ltd., AN045) and the organs isolated using scissors (FST, 14090-09) and forceps (FST, 11018-12). Isolated tissues to be used for mass spectrometry analysis were washed in PBS, weighted, snap-frozen in liquid nitrogen and stored at -80°C. Isolated tissues to be used for immunofluorescence analysis were fixed in 4% formaldehyde, and embedded in paraffin for sectioning using a HistoCore Arcadia H and C (Leica). 4 µm sections were cut using a microm HM 340E (Thermo Fisher) and placed on microscope slides (Menzel, 041300). For subsequent immunofluorescence staining, sections were rehydrated through graded alcohols using a Autostainer XL (Leica) by 2 washes for 10 min in xylene followed by 2 washes in 100% ethanol for 3 min and 1 min each, 1 min wash in 95% ethanol, 1 min wash in 70% ethanol and 50% ethanol (all v/v in water). Next, slides were washed with PBS and following this usual protocol for immunofluorescence was used.

All the procedures were conducted with a protocol approved by animal experiment license NTP-ID 00040377-1-5 (FLI-20-010) in accordance with the guidelines of the 2010/63 EU directive as well as the instructions of GV SOLAS society.

Cell culture and treatments. FlpIn T-REx 293 cells (Thermo Fisher Scientific, R78007), referred to as HEK293T, expressing PSMA4-BirA*, PSMC2-BirA*, SYNJ1-BirA*, BirA*-SYNJ1, BirA*, PSMA4-miniTurbo or miniTurbo were generated as described in (Mackmull et al, 2017). Cells were grown in Dulbecco's modified Eagle's medium (DMEM) high glucose 4.5 g/l supplemented with 10% (v/v) heat inactivated fetal bovine serum (FBS), 2 mM L-Glutamine, 15 µg/ml Blasticidin and 100 µg/ml Hygromycin B. U-2 OS cells (ATCC, HTB-96™; a kind gift from Pospiech lab, Leibniz Institute on Aging- Fritz Lipmann Institute) were grown in the same cell culture medium as FlpIn HEK293 T-REx cells, without antibiotics. All the cells were grown at 37 °C, 5% CO_2 and 95% humidity in a CO_2 incubator. The parental FlpIn T-REx 293 cell line was grown in presence of 100 µg/ml Zeocin™ and 15 µg/ml Blasticidin. Upon generation of stable cell lines, Zeocin™ was replaced by 100 µg/ml Hygromycin B.

For the BioID experiments, HEK293T lines were seeded at the density of approximately 1.6 x 10^4 cells/cm^2 and incubated for 24 h to allow cell attachment to the culture dish. The expression of BirA* or miniTurbo fusion proteins were induced by a single addition of tetracycline stock (solved in ethanol) exposing the cells to its final concentration of 1 µg/µl in total for 4 days. 2 h (miniTurbo lines) or 24 h (BirA* lines) prior to cell harvesting, 50 µM biotin was added to the culture media. For identification of proteasome substrates, PSMA4-miniTurbo or miniTurbo expressing cells were treated with 20 µM MG132 for 4 h and/or 10 µM KB02-JQ1 for 12 h. Upon treatment, cells were washed 3 x times with PBS and harvested by trypsinization. For each sample, a pellet corresponding to 20 million cells was collected and snap-frozen in liquid nitrogen.

Immunoblot. Cell pellets were lysed in 50 mM HEPES pH 7.5, 5 mM EDTA, 150 mM NaCl, 1% (v/v) Triton X-100, prepared with phosphatase inhibitors and protease inhibitors (both from Roche), for 30min on ice. Lysates were cleared by centrifugation for 15 min at 21000 x *g* at 4°C, supernatants transferred to fresh tubes and mixed with loading buffer (1.5 M Tris pH 6.8, 20% SDS (w/v), 85% glycerin (w/v), 5% β-mercaptoethanol (v/v)). This was followed by denaturation for 5 min at 95 °C. 10-20 µg of sample was loaded on a 4–20% Mini-Protean® TGX™ Gels (BIO-RAD) per lane and separated by SDS-PAGE. Proteins were transferred to a nitrocellulose membrane with a Trans-Blot®Turbo™ Transfer Starter System (BioRad, 170-4155) . For high molecular weight samples (SYNJ1-BirA*, and BirA*-SYNJ1) a wet transfer method was used with Hoefer™ TE22 Mini Tank Blotting Unit (Thermo Fisher Scientific, 03-500-216), using a wet transfer buffer (25 mM Tris pH 8.3, 192 mM glycine, 15% (v/v) Methanol).. Membranes were stained with PonceauS for 5 min on a shaker, washed and imaged on a Molecular Imager ChemiDoc™ XRS+ Imaging system (BioRad) and destained. After incubation for 1 h in blocking buffer (3% BSA (w/v), 25 mM Tris, 75 mM NaCl, 0.5% (v/v) Tween-20), membranes were incubated overnight at 4°C with primary antibodies diluted in blocking buffer for FLAG® M2 (1:1000), Streptavidin HRP (1:40000), PSMA4 (1:250), SYNJ1 (1:250), β-actin (1:5000). This was followed by a 1 h incubation with secondary antibodies dilution matching species conjugated with HRP (1:2000, anti-rabbit; 1:1500, anti-mouse, in 0.3% BSA in TBST (w/v)). Proteins were detected using the enhanced chemiluminescence detection kit (ECL) following the manufacturer instructions. Signals were acquired on the Molecular Imager ChemiDoc™XRS+ Imaging system (BioRad).

The immunoblots for anti-FLAG and Streptavidin-HRP on samples from PSMA4-BirA* and PSMC2-BirA*, the cells were lysed in RIPA buffer (150 mM NaCl, 1% Triton X-100 (v/v), 0.5% sodium deoxycholate (w/v), 0.1% SDS (w/v); 50 mM Tris, pH8) prepared with phosphatase

inhibitors and protease inhibitors. Samples were incubated on ice for 10 min and lysates were prepared by sonication in Bioruptor® Plus sonication device (Diagenode). The following steps were performed as indicated previously, but using a different buffer to check the efficiency of the proteins to the membrane (amido black solution (0.25% (w/v), naphthol blue black, 45% (v/v) methanol, 10% (v/v) acetic acid, in milliQ water). After the ECL reaction, membranes were visualized on a CL-XPosure™ Film (Thermo Fisher Scientific, 34090), using an Amersham Hypercassette Autoradiography Cassette (RPN11648).

Proteasome activity assay. The proteasome activity assay (PAA) was performed using the 20S proteasome activity assay kit (Millipore, APT280) following the manufacturer instructions. In short, cell pellets were thawed in ice-cold lysis buffer (50 mM HEPES pH 7.5; 5 mM EDTA; 150 mM NaCl; 1% (v/v) Triton X-100; 2 mM ATP) and left on ice for 30 min with short vortex steps (VWR international, VWR/444-1372) every 10 min. Samples were centrifuged at 20817 x *g*, for 15 min at 4°C to remove any debris. For protein amount estimation the EZQ® Protein Quantitation Kit (Invitrogen, R33200) was used. 50 µg of protein extract were incubated with fluorophore-linked peptide substrate (LLVY-7-amino-4-methylcoumarin, AMC) for 60 min at 37°C. Proteasome activity was measured by quantification of fluorescent units from cleaved AMC at 380/460 nm using a microplate reader m1000 (Tecan).

Size-exclusion chromatography (SEC). Pellets of 80 million HEK293T cells expressing PSMA4-BirA* were collected and snap frozen in liquid nitrogen. The pellets were resuspended in 2 ml lysis buffer (50 mM HEPES pH 6.8; 1 mM MgCl2; 1 mM DTT; 20 mM NaCl; 5% glycerol; phosphatase inhibitors and protease inhibitors) and incubated 30 min on ice. Cell swelling and lysis was checked in 15 min intervals. Cell lysis was assisted by passage of the sample through a 27 G needle 12 times. Following this, the final concentration of NaCl was adjusted to 150 mM. The samples were then clarified by subsequent centrifugation steps as follows: (i) 500 x g for 5 min at 4°C, (ii) 1000 x g for 13 min at 4°C, and (iii) 100000 x g for 30 min at 4°C. The final supernatant was concentrated using 30 kDa cut-off spin filters (Merck Amicon Ultra −0.5 ml, centrifugal filters, UFC503096) to a final protein concentration of approximately 10 µg/µl measured by OD280, and further applied to size-exclusion chromatography.

Size-exclusion chromatography (SEC) was performed using an ÄKTA avant (GE Äkta avant 25-1) system equipped with UV detection at 280 nm wavelength. A Yarra-SEC-4000 column (300 × 7.8 mm, pore size 500 Å, particle size 3 µm) was used with a SecurityGard™ cartridge GFC4000 4 ×

3.0 mm ID as a guard column. Running conditions were 4°C, a flow rate of 0.5 ml/min and run time of 40 min. The mobile phase contained 50 mM HEPES, pH 6.8, 1 mM MgCl2, 1 mM DTT, 150 mM NaCl, and 5 mM ATP. A control sample (Phenomenex) was injected prior to each sample to verify column performance. 100 µl samples from 10 mg/ml lysate solution were injected, corresponding to 1 mg protein extract on column. Fractions (200 µl each) were collected along with the LC separation directly in the SDS buffer, to a final concentration of 4%. Thirty-six fractions were further processed for LC-MS/MS analysis. Of these 36 fractions the first and last two fractions were pooled.

Preparation of SEC fractions for mass spectrometry analysis. The SEC fractions were further processed by addition of DTT (50 mM) in 100 mM HEPES at pH 8, boiled for 5 min at 95°C, followed by sonication (Diagenode Bioruptor® Plus) for 10 cycles (30 s on/60 s off) at 4°C. The samples were then centrifuged at 3000 x g for 5 min at room temperature, and the supernatant transferred to 2 ml tube. This was followed by alkylation with 20 mM iodoacetamide (IAA) for 30 min at room temperature in the dark. Protein amounts were confirmed by SDS–PAGE (4%). Protein samples in the collected fractions ranged from 10 - 100 µg. Proteins were precipitated overnight at −20°C after addition of a 4 × volume of ice-cold acetone. Thereafter, the samples were centrifuged at 20800 x g for 30 min at 4°C and the supernatant carefully removed. Pellets were washed twice with 1 ml ice-cold 80% (v/v) acetone and then centrifuged with 20800 x g at 4°C. The samples were air-dried before addition of 120 µl of digestion buffer (3 M urea; 100 mM HEPES, pH8). Samples were resuspended by sonication (as above) and LysC was added at 1:100 (w/w) enzyme:protein ratio. The samples were then digested for 4 h at 37°C (1000 rpm for 1 h, then 650 rpm, Eppendorf ThermoMixer®C). Samples were then diluted 1:1 with milliQ water, and trypsin added at the same enzyme to protein ratio. Samples were further digested overnight at 37°C (650 rpm). Consequently, digests were acidified by the addition of TFA to a final concentration of 2% (v/v) and then desalted with Waters Oasis® (HLB µElution Plate 30µm, Waters Corporation, Milford, MA, USA) with slow vacuum. Therefore, the columns were conditioned three times with 100 µl solvent B (80% (v/v) acetonitrile; 0.05% (v/v) formic acid and equilibrated three times with 100 µl solvent A (0.05% (v/v) formic acid in Milli-Q water). The samples were loaded, washed 3 times with 100 µl solvent A, and then eluted with 50 µl solvent B. The eluates were dried in a vacuum concentrator.

BioID affinity purification. Cell pellets were thawed on ice were resuspended in 4.75 ml of BioID lysis buffer (50 mM Tris pH 7.5; 150 mM NaCl; 1 mM EDTA; 1mM EGTA; 1% (v/v) Triton

X-100; 1 mg/ml aprotinin; 0.5 mg/ml leupeptin; 250 U turbonuclease; 0.1% (w/v) SDS), followed by 1 h incubation in the rotator mixer (STARLAB RM Multi-1) (15 rpm) at 4°C to aid the lysis. Samples were then briefly sonicated in a Bioruptor Plus for 5 cycles (30 s ON/30 s OFF) at high setting and afterwards centrifuged at 20817 x *g*, for 30 min at 4°C to remove any debris.

Mouse organs were thawed and transferred into Precellys® lysing kit tubes (Keramik-kit 1.4/2.8 mm, 2 ml (CKM)) containing 1 ml of PBS supplemented with 1 tab of cOmplete™, Mini, EDTA-free Protease Inhibitor per 50 ml. For homogenization, organs were shaken twice at 6000 rpm for 30 s using Precellys® 24 Dual (Bertin Instruments, Montigny-le-Bretonneux, France), centrifuged at 946 x *g* at 4°C for 5 min, and the resulting homogenate was transferred to a new tube. Based on the estimated protein content (5% of fresh tissue weight for liver and brain, 8% for heart and kidney and 20% for muscle), homogenates corresponding to 4 mg protein were processed for further BioID affinity purification. This entailed cell lysis of the homogenates by means of BioID lysis buffer.

Streptavidin coated Sepharose beads were acetylated by two successive treatments with 10 mM Sulfo-NHS-Acetate for 30 min at room temperature. The reaction was then quenched with 1M Tris pH 7.5 (1:10 v/v) and then the beads were washed with 1 x PBS and centrifuged at 2000x *g* for 1 min at room temperature. This washing was performed 3 times in total. Cleared lysates were transferred to new tubes, 50 µl of acetylated beads added, and samples were incubated for 3 h on the rotator (15 rpm) at 4°C. This was followed by centrifugation at 2000 x *g* for 5 min at 4°C and removal of 4.5 ml of the supernatant from each sample. Remaining sample with the beads at the bottom was transferred to a Pierce Spin Column Snap Cap column (Thermo Fisher Scientific, 69725) and the tubes were additionally rinsed with lysis buffer and added to the Pierce Spin Column Snap Cap column. Beads were then washed on the column with a lysis buffer, followed by 3 washes with freshly prepared 50 mM ammonium bicarbonate (AmBic), pH 8.3. The bottom of the column was closed with a plug and beads transferred to fresh 2 ml tubes by means of 3 x 300 µl 50 mM AmBic, pH 8.3. The samples were then centrifuged at 2000 x *g* for 5 min at 4°C and the content of each tube was removed until around 200 µl of the liquid (including the bead) remained at the bottom. 1 µg of LysC was added and incubated at 37°C for 16 h shaking at 500 x rpm. The samples were then centrifuged at 2000 x *g* for 5 min at room temperature and the content of the tubes were transferred to Pierce Spin Column Snap Cap columns. The digested peptides were eluted with two times 150 µl of freshly made 50 mM AmBic. To elute biotinylated peptides still bound to the beads, 150 µl of 80% ACN and 20% TFA was added, briefly mixed, and rapidly eluted. This elution step was repeated twice, and the eluates merged. Following

elution, 0.5 µg of trypsin was added to the AmBic elutions and digestion continued for an additional 3 h with mixing at 500 x rpm and 37°C. Digested AmBic elutions were then dried down in a vacuum concentrator, resuspended in 200 µl 0.05% (v/v) formic acid in milliQ water and sonicated in a Bioruptor Plus (5 cycles with 1 min ON and 30 s OFF with high intensity at 20°C). ACN/TFA elutions were dried down in a vacuum concentrator (not to completeness but until approximately 50 µl were left), 50 µl of 200 mM HEPES pH 8.0 were added to the samples and pH adjusted to 7-9. 0.5 µg of trypsin were then added and digestion continued for an additional 3 h with mixing at 500 x rpm and 37°C. Digested peptides were acidified with 10% (v/v) trifluoroacetic to pH <3. Both AmBic and ACN/TFA elutions were desalted using Macro Spin Column C18 columns following manufacturer's instructions and dried down in a vacuum concentrator.

Preparation of whole proteome samples from mouse organs for mass spectrometry analysis. Mouse organ lysates containing 100 µg of total proteins were processed by acetone precipitation and protein digestion as described in "Preparation of SEC fractions for mass spectrometry analysis".

LC-MS/MS data acquisition. *LC (liquid chromatography).* Prior to analysis, samples were reconstituted in in MS Buffer (5% acetonitrile, 95% Milli-Q water, with 0.1% formic acid) and spiked with iRT peptides (Biognosys, Switzerland). Peptides were separated in trap/elute mode using the nanoAcquity MClass Ultra-High Performance Liquid Chromatography system (UPLC) or nanoAcquity UPLC system (Waters, Waters Corporation, Milford, MA, USA) equipped with a trapping (nanoAcquity Symmetry C18, 5 µm, 180 µm × 20 mm) and an analytical column (nanoAcquity BEH C18, 1.7 µm, 75 µm × 250 mm). Solvent A was water and 0.1% formic acid, and solvent B was acetonitrile and 0.1% formic acid. 1 µl of the sample (～1 µg on column) were loaded with a constant flow of solvent A at 5 µl/min onto the trapping column. Trapping time was 6 min. Peptides were eluted via the analytical column with a constant flow of 0.3 µl/min. During the elution, the percentage of solvent B increased in a nonlinear fashion from 0–40% in 90 min (120 min for total proteome of mouse organs). Total run time was 115 min (145 min) including equilibration and conditioning. The LC was coupled to an Orbitrap Fusion Lumos (Thermo Fisher Scientific, Bremen, Germany) using the Proxeon nanospray source or to an Orbitrap Q-Exactive HFX (Thermo Fisher Scientific) for BioID experiments from HEK293T cells, or to an Orbitrap Exploris 480 (Thermo Fisher Scientific, Bremen, Germany) for BioID experiments combined with PROTAC treatment. The peptides were introduced into the mass spectrometer via a Pico-Tip

Emitter 360-µm outer diameter × 20-µm inner diameter, 10-µm tip (New Objective) heated at 300 °C, and a spray voltage of 2.2 kV was applied. For data acquisition and processing of the raw data Tune version 2.1 and Xcalibur 4.1 (Orbitrap Fusion Lumos), Tune 2.9 and Xcalibur 4.0 (Orbitrap Q-Exactive HFX) and Tune 3.1 and Xcalibur 4.4 (Orbitrap Exploris 480) were employed.

DDA (Data-dependent acquisition). SEC fractions, mouse BioID as well as BioID of PSMA4 and PSMC2 were analyzed using DpD (DDA plus DIA). Here, data from a subset of conditions were first acquired in DDA mode to contribute to a sample specific spectral library. Full scan MS spectra with mass range 375-1500 m/z (using quadrupole isolation) were acquired in profile mode in the Orbitrap with resolution of 60,000 FWHM. The filling time was set at a maximum of 50 ms with a limitation of 2 x 10^5 ions. The "Top Speed" method was employed to take the maximum number of precursor ions (with an intensity threshold of 5 x 10^5) from the full scan MS for fragmentation (using HCD collision energy, 30%) and quadrupole isolation (1.4 Da window) and measurement in the Orbitrap, with a cycle time of 3 seconds. The MIPS (monoisotopic precursor selection) peptide algorithm was employed. MS/MS data were acquired in centroid mode in the Orbitrap, with a resolution of 15,000 FWHM and a fixed first mass of 120 m/z. The filling time was set at a maximum of 22 ms with a limitation of 1 x 10^5 ions. Only multiply charged (2+ - 7+) precursor ions were selected for MS/MS. Dynamic exclusion was employed with maximum retention period of 15 s and relative mass window of 10 ppm. Isotopes were excluded.

DIA (Data-dependent acquisition). The DIA data acquisition was the same for both directDIA and DpD. Full scan mass spectrometry (MS) spectra with mass range 350–1650 m/z were acquired in profile mode in the Orbitrap with resolution of 120,000 FWHM. The default charge state was set to 3+. The filling time was set at a maximum of 60 ms with a limitation of 3 × 10^6 ions. DIA scans were acquired with 34 mass window segments of differing widths across the MS1 mass range. Higher collisional dissociation fragmentation (stepped normalized collision energy; 25, 27.5, and 30%) was applied and MS/MS spectra were acquired with a resolution of 30,000 FWHM with a fixed first mass of 200 m/z after accumulation of 3 × 10^6 ions or after filling time of 35 ms (whichever occurred first). Data were acquired in profile mode.

LC-MS/MS data analysis. DpD (DDA plus DIA) libraries were created by searching both the DDA runs and the DIA runs using Spectronaut Pulsar (v 13-15, Biognosys, Zurich, Switzerland). The data were searched against species specific protein databases (*Homo sapiens*, reviewed entry only (16,747 entries), release 2016_01 or *Mus musculus*, entry only (20,186), release 2016_01 respectively) with a list of common contaminants appended. The data were searched

with the following modifications: carbamidomethyl (C) as fixed modification, and oxidation (M), acetyl (protein N-term), and biotin (K) as variable modifications. A maximum of 2 missed cleavages was allowed. The library search was set to 1% false discovery rate (FDR) at both protein and peptide levels. This library contained 79,732 precursors, corresponding to 4,730 protein groups for SEC fractions, 77,401 precursors, corresponding to 5,125 protein groups for BioID on PSMA4 and PSMC2 and 67,490 precursors, corresponding to 4,525 protein groups for mouse BioID using Spectronaut protein inference. All other BioID and mouse proteome experiments were processed using the directDIA pipeline in Spectronaut Professional (v.13-15). The data were searched against a species specific (*Mus musculus* and *Homo sapiens*, as described above) with a list of common contaminants appended. BGS factory settings were used with the exception of: variable modifications = acetyl (protein N-term), biotin (K), oxidation (M).

SEC-MS experiments were processed using Spectronaut v.13 with default settings except: Proteotypicity Filter = Only Protein Group Specific; Major Group Quantity = Median peptide quantity; Major Group Top N = OFF; Minor Group Quantity = Median precursor quantity; Minor Group Top N = OFF; Data Filtering = Qvalue sparse; Imputing Strategy = No imputing; Cross run normalization = OFF.

PSMA4 and PSMC2 BioID experiments were processed using Spectronaut v.13 with default settings except: Proteotypicity Filter = Only Protein Group Specific; Major Group Quantity = Median peptide quantity; Major Group Top N = OFF; Minor Group Quantity = Median precursor quantity; Minor Group Top N = OFF; Data Filtering = Qvalue percentile (0.5); Imputing Strategy = No imputing; Normalization Strategy = Global Normalization; Normalize on = Median; Row Selection = Qvalue sparse.

SYNJ1 BioID experiments were processed using Spectronaut v.13 with default settings except: Proteotypicity Filter = Only Protein Group Specific; Major Group Quantity = Median peptide quantity; Major Group Top N = OFF; Minor Group Quantity = Median precursor quantity; Minor Group Top N = OFF; Data Filtering = Qvalue percentile (0.5); Imputing Strategy = No imputing; Normalization Strategy = Global Normalization; Normalize on = Median; Row Selection = Qvalue complete.

Mouse BioID and BioID experiments combined with PROTAC treatment were processed using Spectronaut v.15 with default settings except: Proteotypicity Filter = Only Protein Group Specific; Major Group Quantity = Median peptide quantity; Major Group Top N = OFF; Minor Group

Quantity = Median precursor quantity; Minor Group Top N = OFF; Data Filtering = Qvalue percentile (0.2); Imputing Strategy = Global imputing; Normalization Strategy = Global Normalization; Normalize on = Median; Row Selection = Qvalue complete.

Mouse proteome data were processed using Spectronaut v.15 with default settings except: Proteotypicity Filter = Only Protein Group Specific; Normalization Strategy = Local Normalization.

For all the BioID experiments, differential abundance testing was performed in Spectronaut using a paired t-test between replicates. P values were corrected for multiple testing multiple testing correction with the method described by Storey [44]. The candidates and protein report tables were exported from Spectronaut and used for volcano plots generation and Principal Component Analysis (PCA), respectively, using R and RStudio server.

Immunofluorescence. Cells were grown on coverslips (Carl Roth, YX03.1) in 12-well plates (Lab solute, 7696791), 25000 cells per well. Cells were washed three times with 1 x PBS, fixed in 4% formaldehyde (v/v) in PBS for 10 min at room temperature, washed 3 x 5 min with 1 x PBS and permeabilized with permeabilization buffer (0.7% Triton X-100; in 1 x PBS) at room temperature for 15 min. Washing with PBS was repeated 2 x 5 min and samples were incubated with blocking solution (10% (w/v) BSA; 10% (v/v) Triton X-100; 5% (v/v) goat serum) for 10 min at room temperature. The coverslips were incubated with primary antibody anti-FLAG®M2 at 4°C overnight (Sigma Aldrich, mouse IgG1, 1:100). After washing 3 x 5 min with PBS/PBST (first with PBS, second with PBS + 0.2% (v/v) Tween 20, third with PBS) the secondary fluorescence-labeled antibody (goat anti-mouse IgG (H+L) - Cyanine5, 1:400 in blocking solution) and fluorescently labeled streptavidin, 1:2000 in blocking solution) were incubated for 30 min at 37°C. After 3 x 5 min with PBS/PBST (first with PBS, second with PBS + 0.2% (v/v) Tween 20, third with PBS), nuclei were stained with DAPI (4',6-Diamidino-2-Phenylindole, Dihydrochloride, 0.02 µg/µl in PBS) at room temperature for 10 min and washed again with PBS 2 x 5 min. Frozen sections and single fibers were mounted in Permafluor mounting medium using glass slides (041300, Menzel) and dried at room temperature overnight. All samples were stored at 4°C in the dark until further analysis by microscopy. Immunofluorescence microscopy was performed with an Axio Imager (Z2 using a Plan-Apochromat 20 x / 0.8 M27 Objective) and analyzed with the software Zen 2 Blue Edition (Carl Zeiss Microscopy GmbH).

Proximity ligation assay (PLA). Cells were grown in 12 well chambers (ibidi, 81201) coated with Poly-D-Lysin, with 5000 cells per well. Cells were washed three times with PBS, fixed in 4%

formaldehyde in PBS for 10 min at room temperature, washed 3 x 5 min with PBS and permeabilized with permeabilization buffer (0.7% Triton X-100; in PBS) at room temperature for 15 min. This was followed by washes of 2 x 5 min with PBS, and samples were incubated with Duolink® Blocking Solution (40 µl per well), for 60 min at 37°C in a humidity chamber. The blocking solution was removed, and cells were incubated at 4°C overnight in a humidity chamber with following primary antibodies: anti-Proteasome 20S alpha 1+2+3+5+6+7 (1:200 in Duolink® Antibody Diluent) and anti -SYNJ1 (1:100 in Duolink® Antibody Diluent). Primary antibody solutions were removed and the slides with the cells were washed 2 x 5 min in Duolink® *In Situ* wash buffer A at room temperature. This was followed by incubation with PLA probe solution (Duolink® *In Situ* PLA® Probe Anti-Mouse MINUS, diluted 1:5 in Duolink® Antibody Diluent and Duolink® *In Situ* PLA® Probe Anti-Rabbit PLUS, diluted 1:5 in Duolink® Antibody Diluent) for 1 hour at 37°C - samples propped up on a rack in a water bath (VWR, VWB18) . The cells were washed 2 x 5 min in Duolink® *In Situ* Wash Buffer A at room temperature, followed by incubation with ligase solution in ligation buffer (Ligase from Duolink® *In Situ* Detection Reagents Red kit, diluted 1:40 in ligation buffer from the same kit) for 30 min at 37°C in a water bath. The cells were washed 2 x 5 min in Duolink® *In Situ* Wash Buffer A at room temperature, followed by incubation with polymerase solution in amplification buffer (Polymerase from Duolink® *In Situ* Detection Reagents Red kit, diluted 1:80 in diluted 5 x Amplification Red buffer from the same kit) for 100min at 37°C in a water bath. Cells were then washed 2 x 10 min in Duolink® *In Situ* Wash Buffer B at room temperature followed by a wash in 0.01 x Duolink® In Situ Wash Buffer B for 1 min at room temperature. The slides with the cells were then mounted with a coverslip (ibidi, 10811) using Duolink® *In Situ* Mounting Medium with DAPI and dried at room temperature overnight. All samples were stored at 4°C in the dark until further analysis with the microscope. Immunofluorescence microscopy was performed with an Axio Imager Z2 using a Plan-Apochromat 20 x / 0.8 M27 Objective (Zeiss).

Molecular visualization and structure analysis. For visualization of proteasome complexes UCSF Chimera program (version 1.13.1) was used. The three-dimensional structural data of macromolecular complexes of proteasome were downloaded from the Protein Data Bank (PDB) database (5T0C). For the analysis of the enrichment of proteasome subunits in BioID protocol, data sets with fold change information were used and filtered the following way: q value < 0.05, number of identified unique peptides per protein ≥ 2. The intensity of the proteasome subunit coloring used was directly dependent on the fold change of the identified subunit in the BioID affinity purification.

Data availability. Mass spectrometry proteomics data have been deposited to the ProteomeXchange Consortium via the PRIDE [45] partner repository and they are accessible with the identifiers:

PXD032833 for the ProteasomeID HEK293T dataset;

PXD034874 for the ProteasomeID HEK293T size exclusion chromatography dataset;

PXD032841 for the SYNJ1 BioID dataset;

PXD033008 for the ProteasomeID MG132 dataset;

PXD032976 for the ProteasomeID PROTAC dataset;

PXD034965 for the ProteasomeID MG132 whole cell proteome dataset;

PXD032811 for the ProteasomeID mouse whole tissue proteome dataset;

PXD032388 for the ProteasomeID mouse dataset.

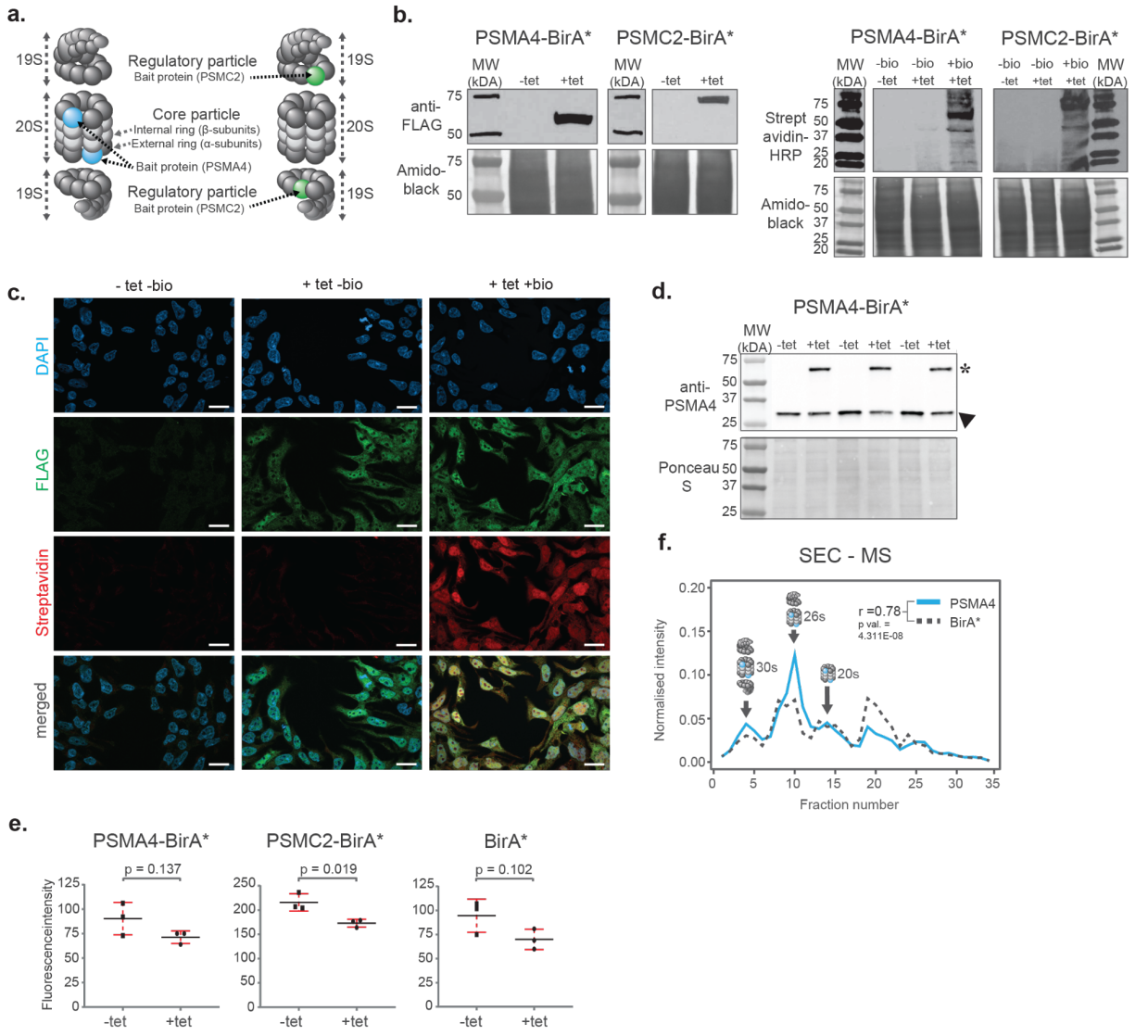

Figure 1: Establishment of a cell culture model system for proximity labeling of proteasomes

a. Schematic representation of proteasome and location of components fused to biotin ligase (bait proteins. shown in blue and green for 20S and 19S proteasome, respectively).

b. Left panel, immunoblot of BirA* fusion proteins performed on lysates from HEK293T cells stably transfected with PSMA4-BirA*-FLAG or PSMC2-BirA*-FLAG following 24h incubation with (+tet) or without (−tet) tetracycline. Right panel, streptavidin-HRP blot following induction of BirA* fusion proteins with tetracycline and supplementation of biotin for 24h. For both panels, Amido Black staining was used as loading control. HRP: horseradish peroxidase.

c. Immunofluorescence analysis of PSMA4-BirA*-FLAG cell line 4 days after seeding without addition of any substance (-tet -bio), with addition of only tetracycline for 4 days (+tet -bio) or with addition of both tetracycline for 4 days and biotin for 1 day (+tet +bio). Scale bar indicates 20µm.

d. Comparison of expression levels of PSMA4-BirA* (lanes marked by star) and its endogenous counterpart (lanes marked by arrowhead), following 24 h incubation with (+tet) or without (−tet) tetracycline. Ponceau S staining was used as loading control.

e. Proteasome activity assay performed on lysates from cell lines expressing different BirA* fusion proteins, following 24 h incubation with (+tet) or without (−tet) tetracycline. Equal amounts of protein extracts were incubated with proteasome substrate LLVY-7-Amino-4-methylcoumarin (AMC) and substrate cleavage assessed by fluorimetry. n = 3 biological replicates, paired t-test.

f. Size exclusion chromatography (SEC) analysis of lysates from HEK293T cells stably expressing PSMA4-BirA* following 24 h incubation with tetracycline. SEC fractions were analyzed by DIA mass spectrometry and elution profiles were built for each protein using protein quantity values normalized to the sum of quantities across all fractions. Depicted are elution profiles of PSMA4 (proteasome subunit, blue) and BirA* (biotinylating enzyme, dashed line). The peaks corresponding to different proteasome assemblies were assigned based on the elution profiles of other proteasome components.

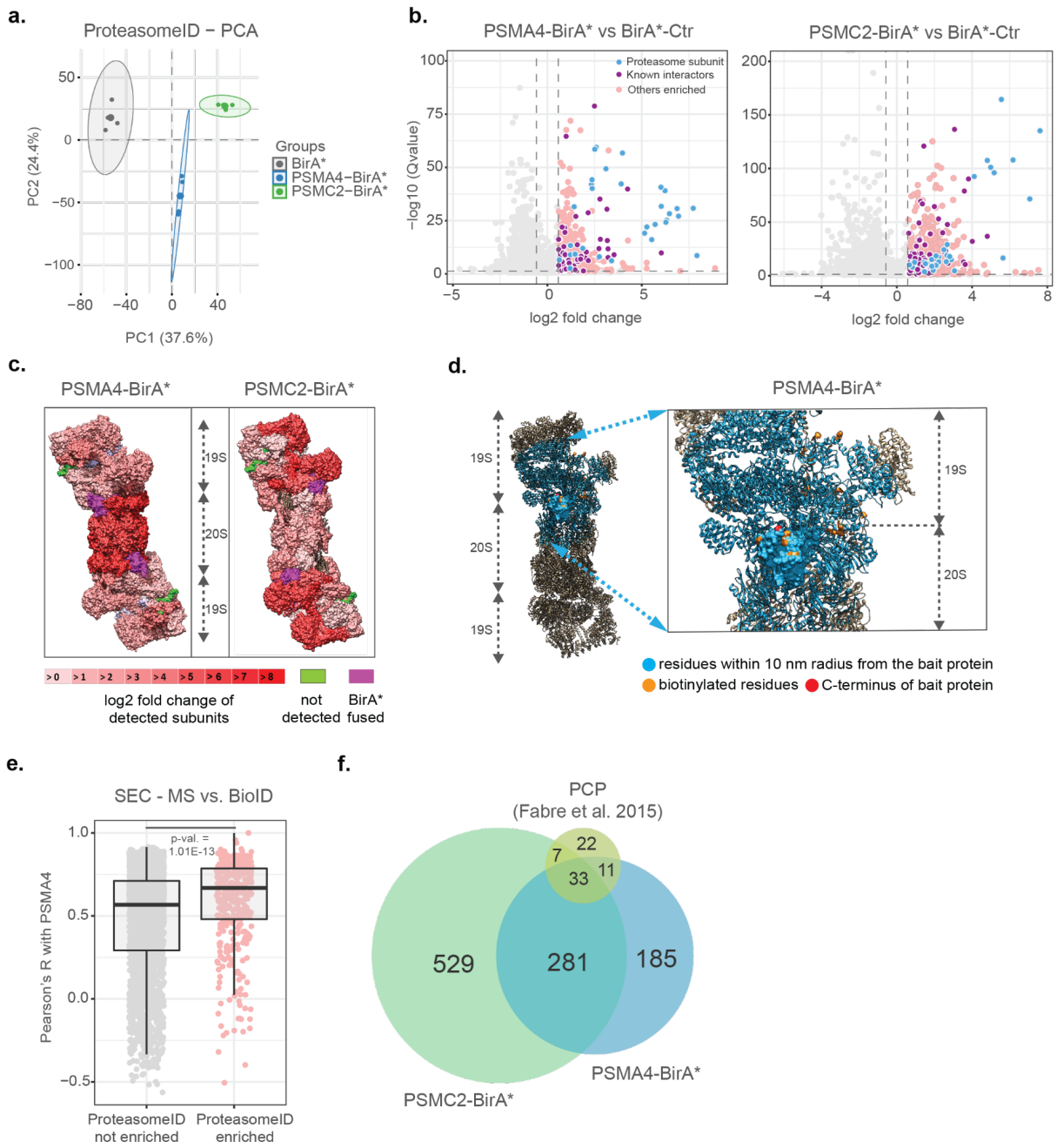

Figure 2: Validation of ProteasomeID

a. PCA of BioID data obtained from cell lines expressing BirA*-fused proteasome subunits and control (BirA*). The smaller dots represent individual samples and the larger dots the centroids of each group. Ellipses represent 95% confidence intervals. The percentage of variance explained by the first two principal components (PC) axes is reported in the axis titles. n = 4, biological replicates.

b. Volcano plots of proteins enriched by streptavidin pull-down and analyzed by DIA mass spectrometry. Cut offs for enriched proteins: log2 fold change > 1 and Q value < 0.05. n = 4, biological replicates.

c. Level of enrichment of proteasome subunits measured by ProteasomeID in the context of the proteasome structure. Enriched proteins are depicted in different shades of red according to the log2 fold enrichment vs. BirA* control.

d. Biotinylated protein sites identified by ProteasomeID. Highlighted in blue are all residues located within a 10 nm radius of the BirA*-modified PSMA4 subunit. Only the structure of the modified subunit is depicted with a surface model and all the other subunits are depicted as helix-loop structures. Red color indicates the C-terminus of PSMA4 and the identified biotinylated residues are depicted in orange. Biotinylated residues were obtained from the ACN fraction of PSMA4-BirA*. The proteasome structures depicted in c. and d. were obtained from the PDB:5T0C model of the human 26S proteasome [46] and rendered using Chimera [47].

e. Comparison of co-elution profiles obtained by SEC-MS and proteins enriched in ProteasomeID. Pearson correlation values were calculated between PSMA4 and all the other proteins quantified in SEC-MS (n=4680). Correlation values were compared between proteins significantly enriched in PSMA4-BirA* vs. BirA* (log2 fold change > 1 and Q value < 0.05) and all the other proteins quantified in the ProteasomeID experiment. P value was calculated using a Wilcoxon Rank Sum test with continuity correction.

f. Venn diagram showing the overlap between proteins significantly enriched in ProteasomeID and proteasome-interacting proteins identified by Protein Correlation Profiling (PCP) in an independent study [25]. ProteasomeID data were filtered for log2 fold change > 1 and Q value < 0.05 vs. BirA* control.

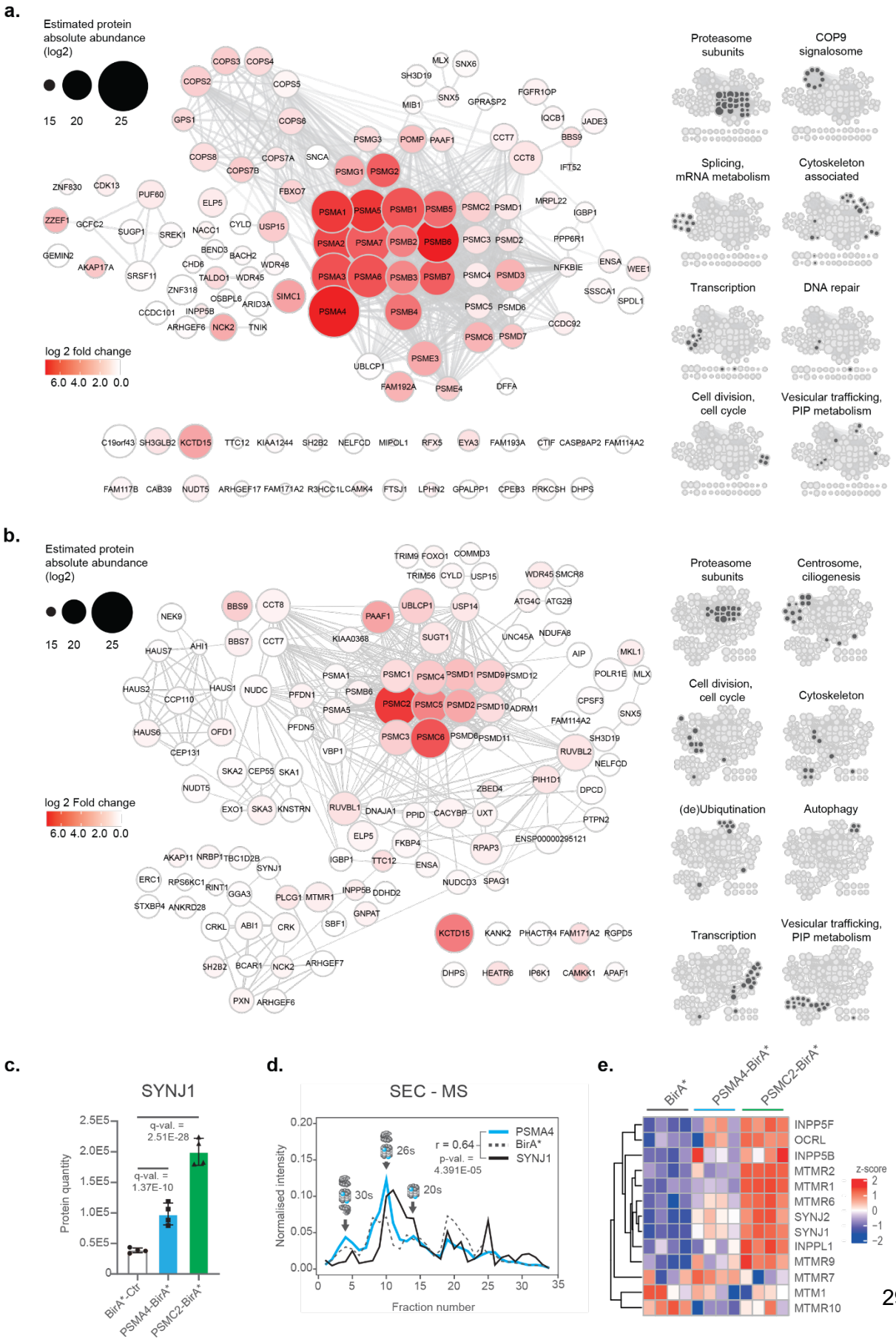
a.
Estimated protein absolute abundance (log2)
15 20 25
log 2 fold change
6.0 4.0 2.0 0.0
Proteasome subunits
COP9 signalosome
Splicing, mRNA metabolism
Cytoskeleton associated
Transcription
DNA repair
Cell division, cell cycle
Vesicular trafficking, PIP metabolism
b.
Estimated protein absolute abundance (log2)
15 20 25
log 2 Fold change
6.0 4.0 2.0 0.0
Proteasome subunits
Centrosome, ciliogenesis
Cell division, cell cycle
Cytoskeleton
(de)Ubiqutination
Autophagy
Transcription
Vesicular trafficking, PIP metabolism
c.
SYNJ1
Protein quantity
q-val. = 2.51E-28
q-val. = 1.37E-10
BirA*-Ctr
PSMA4-BirA*
PSMC2-BirA*
d.
SEC - MS
Normalised intensity
Fraction number
r = 0.64
p-val. = 4.391E-05
PSMA4
BirA*
SYNJ1
26s
30s
20s
e.
BirA*
PSMA4-BirA*
PSMC2-BirA*
INPP5F
OCRL
INPP5B
MTMR2
MTMR1
MTMR6
SYNJ2
SYNJ1
INPPL1
MTMR9
MTMR7
MTM1
MTMR10
z-score

Figure 3: ProteasomeID identifies potential novel interactors of the proteasome

a., b. Network analysis of top 125 interactors of PSMA4-BirA* (a.) and PSMC2-BirA* (b.) obtained by ProteasomeID. Identified proteins were filtered for significance (Q value < 0.05) and then sorted according to the log2 fold changes of enrichment vs. BirA* control cell line. The size of the nodes depicts the median protein quantity across samples (an estimate of protein absolute abundance), while the color indicates the log2 fold change vs. BirA* control. The right panel highlights groups of proteins belonging to the same protein complex or biological process.

c. Barplot comparing the levels of SYNJ1 protein following streptavidin enrichment from different cell lines. Protein quantities were derived from DIA mass spectrometry data. Q values were obtained from a paired *t* test corrected from multiple testing as implemented in the Spectronaut software (see Methods). n = 4 biological replicates.

d. SEC-MS analysis comparing elution profiles of PSMA4 (blue), BirA* (dashed gray) and SYNJ1 (black). SEC fractions were obtained from lysates of HEK293T cells expressing PSMA4-BirA* and analyzed by DIA mass spectrometry. Elution profiles were built for each protein using protein quantity values normalized to the sum of quantities across all fractions.

e. Heatmap showing the relative abundance of phospho-inositol phosphatases quantified in ProteasomeID samples. Protein quantities obtained from DIA mass spectrometry were z-transformed for display purposes.

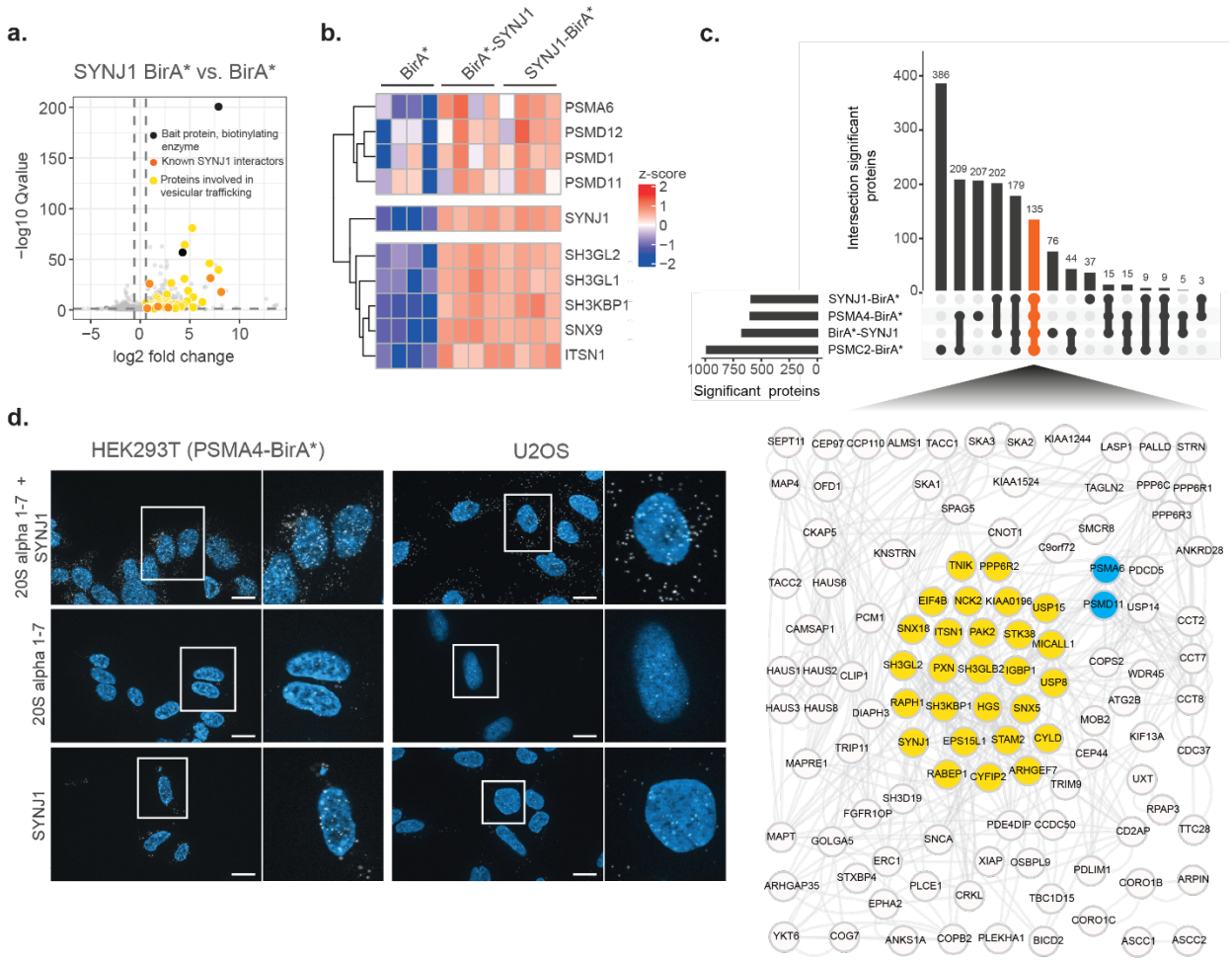

Figure 4: ProteasomeID identifies SYNJ1 protein as novel interactor

a. Volcano plot of proteins enriched by streptavidin pull-down and analyzed by DIA mass spectrometry from SYNJ1-BirA* and BirA* control cell lines. Cut offs for enriched proteins: log2 fold change > 1 and Q value < 0.05. n = 4, biological replicates.

b. Heatmap showing the relative abundance of SYNJ1 (bait protein), known SYNJ1-interacting proteins, and proteasome subunits found to be enriched (log2 fold change > 1 and Q value < 0.05) in ProteasomeID samples from either SYNJ1-BirA* or BirA*-SYNJ1- vs. BirA* control. Protein quantities obtained from DIA mass spectrometry were z-transformed for display purposes.

c. Overlap of significantly enriched proteins (log2 fold change > 1 and Q value < 0.05) in proteasome and SYNJ1 BioID samples vs. BirA* control. Proteins found to be enriched in all the proteasome and SYNJ1 samples are highlighted in a network representation. Nodes colored in yellow indicate a group of proteins related to vesicular transport. Nodes highlighted in blue are proteasome subunits.

d. Immunofluorescence analysis of PLA experiment performed on PSMA4-BirA* cell after 24 h incubation with 1µg/ml tetracycline, as well as on U2OS cells. Scale bar indicates 20µm.

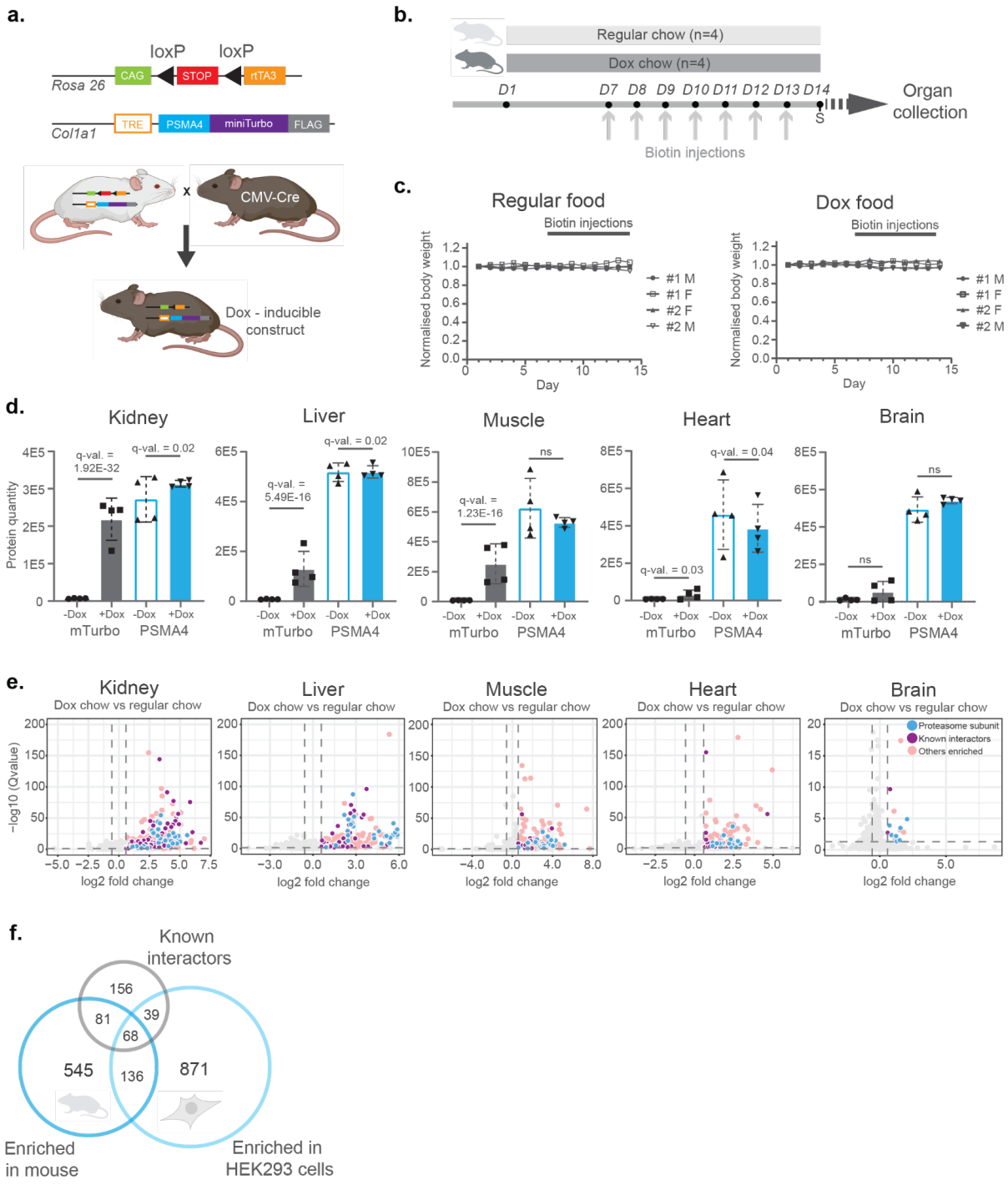

Figure 5: Establishment of a mouse model for *in vivo* ProteasomeID

a. Design of a mouse model for ProteasomeID. The lox-STOP-lox cassette was excised from the Rosa26 locus by crossing with a mouse line expressing the Cre recombinase under the control of an ubiquitous CMV promoter [33]. CAG: CAG promoter [48], TRE: tetracycline-regulated element; rtTA3: reverse tetracycline-dependent transactivator A3 [32]. (Figure created with biorender)

b. Scheme of *in vivo* ProteasomeID experiment. D: day, S: sacrifice.

c. Bodyweight curves of the experimental animals. The body weight for each mouse was normalized to its value at day 1 of the experiment (set to 1). M: male, F: female.

d. Barplot comparing the protein levels of miniTurbo (gray bars) and PSMA4 (light blue bars) in organs of mice fed with regular chow (-Dox, open bars) or doxycycline-containing food (+Dox, filled bars). Protein quantities were derived from DIA mass spectrometry data obtained from whole organ lysates. Q values were obtained from a paired *t* test corrected from multiple testing as implemented in the Spectronaut software (see Methods). n = 4, animals per experimental group.

e. Volcano plots of proteins enriched by streptavidin pull-down and analyzed by DIA mass spectrometry from different mouse organs. Cut offs for enriched proteins: log2 fold change > 1 and Q value < 0.05. n = 4, animals per experimental group.

f. Venn diagram showing the overlap between proteins significantly enriched in ProteasomeID samples from mouse organs, HEK293T cells (either PSMA4-BirA* or PSMC2-BirA*), and proteasome-interacting proteins retrieved from the literature (Table S6). ProteasomeID data were filtered for log2 fold change > 1 and Q value < 0.05 vs. BirA* or miniTurbo control.

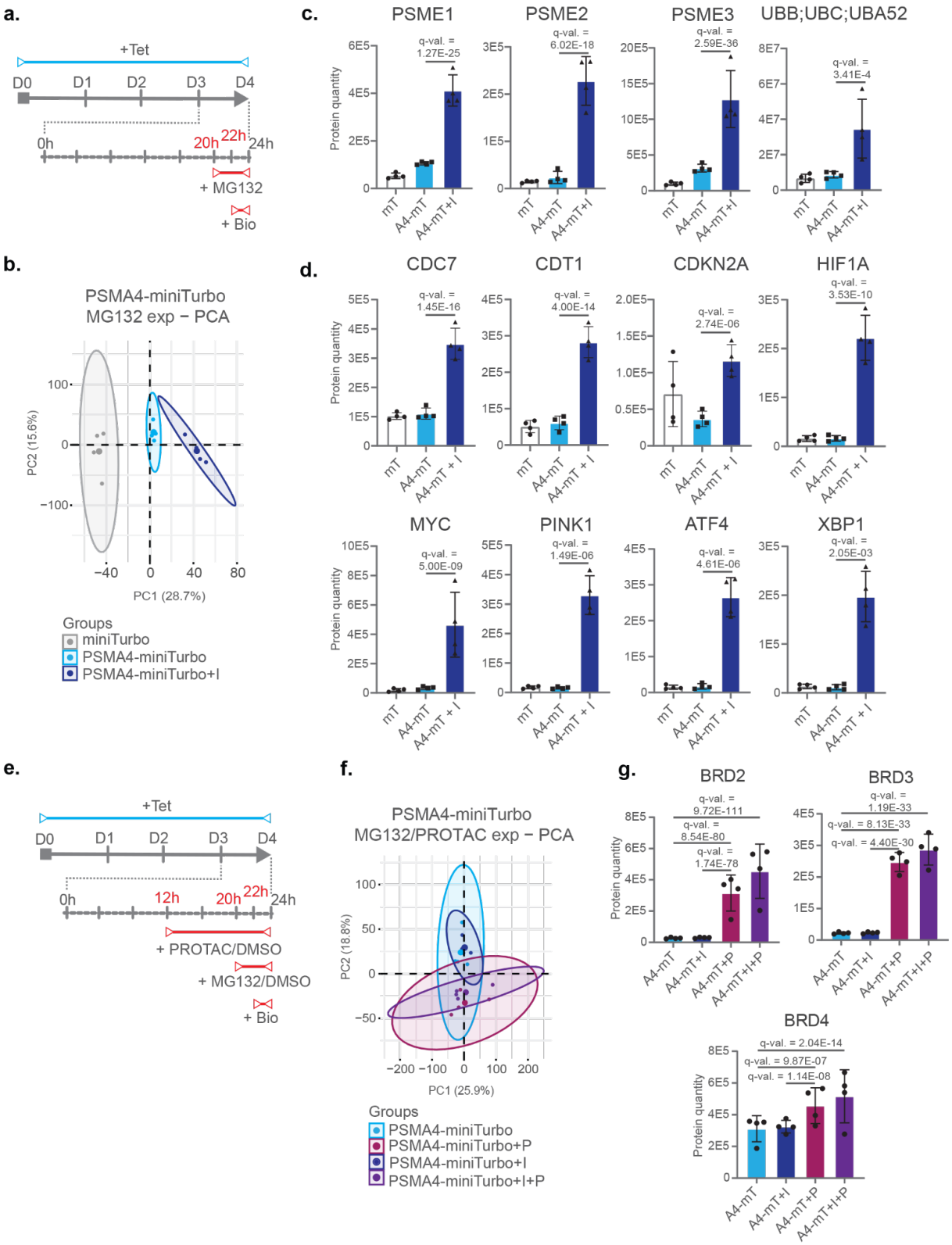
a.
+Tet
D0
D1
D2
D3
D4
0h
20h
22h
24h
+ MG132
+ Bio
b.
PSMA4-miniTurbo
MG132 exp − PCA
PC2 (15.6%)
PC1 (28.7%)
Groups
miniTurbo
PSMA4-miniTurbo
PSMA4-miniTurbo+I
c.
PSME1
PSME2
PSME3
UBB;UBC;UBA52
Protein quantity
q-val. = 1.27E-25
q-val. = 6.02E-18
q-val. = 2.59E-36
q-val. = 3.41E-4
mT
A4-mT
A4-mT+I
d.
CDC7
CDT1
CDKN2A
HIF1A
MYC
PINK1
ATF4
XBP1
q-val. = 1.45E-16
q-val. = 4.00E-14
q-val. = 2.74E-06
q-val. = 3.53E-10
q-val. = 5.00E-09
q-val. = 1.49E-06
q-val. = 4.61E-06
q-val. = 2.05E-03
A4-mT + I
e.
+Tet
D0
D1
D2
D3
D4
0h
12h
20h
22h
24h
+ PROTAC/DMSO
+ MG132/DMSO
+ Bio
f.
PSMA4-miniTurbo
MG132/PROTAC exp − PCA
PC2 (18.8%)
PC1 (25.9%)
Groups
PSMA4-miniTurbo
PSMA4-miniTurbo+P
PSMA4-miniTurbo+I
PSMA4-miniTurbo+I+P
g.
BRD2
BRD3
BRD4
q-val. = 9.72E-111
q-val. = 8.54E-80
q-val. = 1.74E-78
q-val. = 1.19E-33
q-val. = 8.13E-33
q-val. = 4.40E-30
q-val. = 2.04E-14
q-val. = 9.87E-07
q-val. = 1.14E-08
A4-mT
A4-mT+I
A4-mT+P
A4-mT+I+P

Figure 6: ProteasomeID identifies endogenous and PROTAC-induced proteasome substrates

a. Scheme of ProteasomeID workflow in HEK293T cells including proteasome inhibition by MG132. PSMA4-miniTurbo expression and incorporation into proteasomes is achieved by 4 day induction with tetracycline. Proteasome inhibition is achieved by addition of 20µM MG132 4 h before the cell harvesting. Biotin substrate for miniTurbo is supplied 2 h before the cell harvesting. D: day; h: hour; Tet: tetracycline; Bio: biotin.

b. PCA of BioID data obtained from cell lines expressing PSMA4-miniTurbo and control (miniTurbo), and PSMA4-miniTurbo following exposure to proteasome inhibitor MG132. The smaller dots represent individual samples and the larger dots the centroids of each group. Ellipses represent 95% confidence intervals. The percentage of variance explained by the first two principal components (PC) axes is reported in the axis titles. n = 4, biological replicates.

c., d. Barplots comparing the levels of proteasome activators and ubiquitin (c.), and known proteasome substrates (d.) following streptavidin enrichment from different cell lines and following proteasome inhibition by MG132. Protein quantities were derived from DIA mass spectrometry data. Q values were obtained from a paired *t* test corrected from multiple testing as implemented in the Spectronaut software (see Methods). n = 4 biological replicates. mT: miniTurbo control cell line; A4-mT: PSMA4-miniTurbo cell line; I: proteasome inhibition by MG132

e. Scheme of ProteasomeID workflow in HEK293T cells including proteasome inhibition by MG132 and treatment with PROTAC KB02-JQ1. The experimental design is analogous to the one depicted in (a.) with the additional PROTAC treatment achieved by addition of 10µM KB02-JQ1 12 h before cell harvesting. D: day; h: hour; Tet: tetracycline; Bio: biotin.

f. PCA of BioID data obtained from cells expressing PSMA4-miniTurbo exposed to the proteasome inhibitor MG132 and/or the PROTAC KB02-JQ1. The smaller dots represent individual samples and the larger dots the centroids of each group. Ellipses represent 95% confidence intervals. The percentage of variance explained by the first two principal components (PC) axes is reported in the axis titles. n = 4, biological replicates.

g. Barplots comparing the levels of BRD-containing proteins following streptavidin enrichment from PSMA4-miniTurbo expressing cells exposed to the proteasome inhibitor MG132 and/or the PROTAC KB02-JQ1. Q values were obtained from a paired *t* test corrected from multiple testing as implemented in the Spectronaut software (see Methods). n = 4 biological replicates. mT: miniTurbo control cell line; A4-mT: PSMA4-miniTurbo cell line; I: proteasome inhibition by MG132; P: PROTAC (KB02-JQ1).

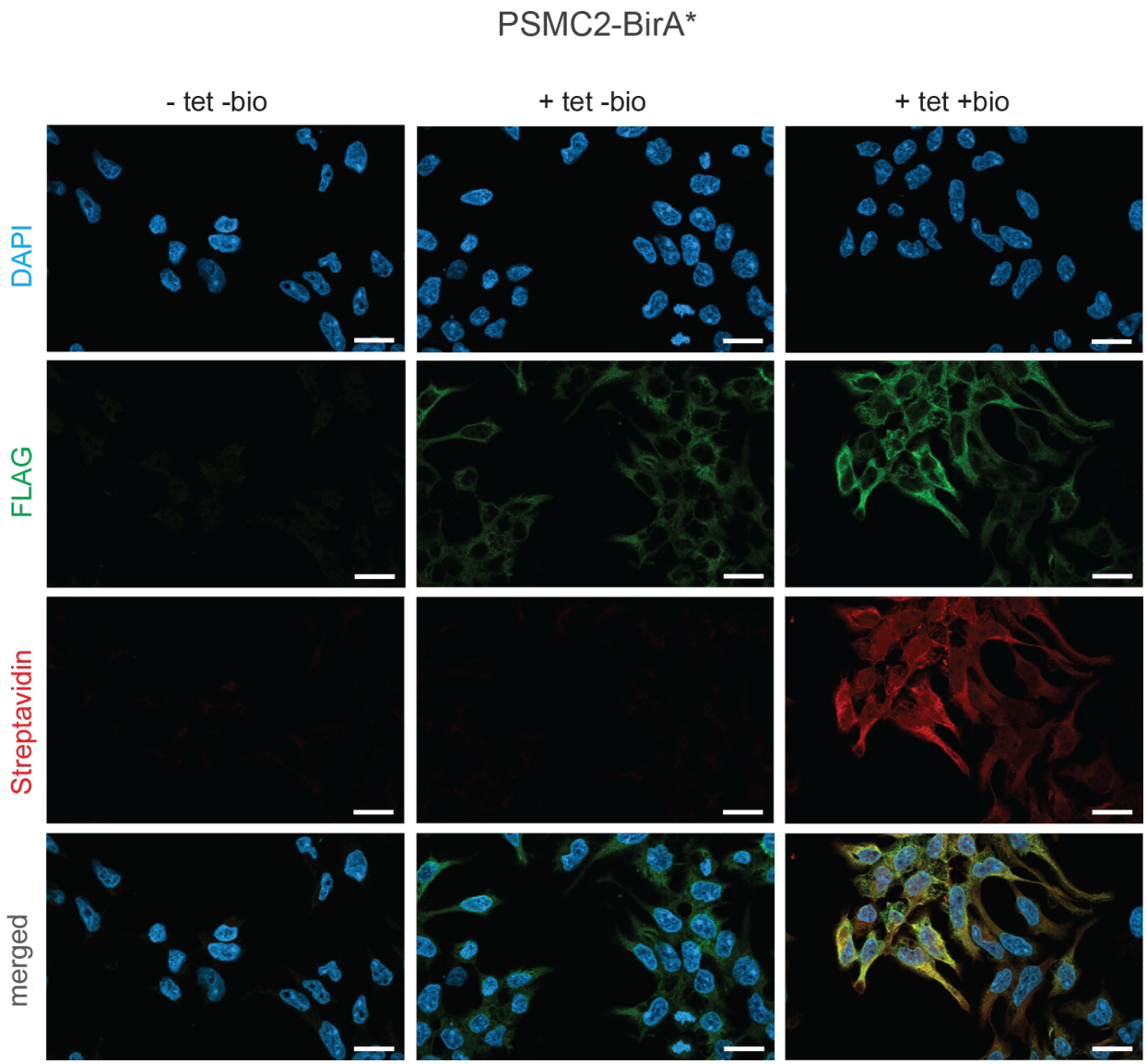

Supplemental figure 1: Immunofluorescence validation of PSMC2-BirA* expressing cell line

Immunofluorescence analysis of PSMC2-BirA*-FLAG cell line 4 days after seeding without addition of any substance (-tet -bio), with addition of only tetracycline for 4 days (+tet -bio) or with addition of both tetracycline for 4 days and biotin for 1 day (+tet +bio). Scale bar indicates 20µm.

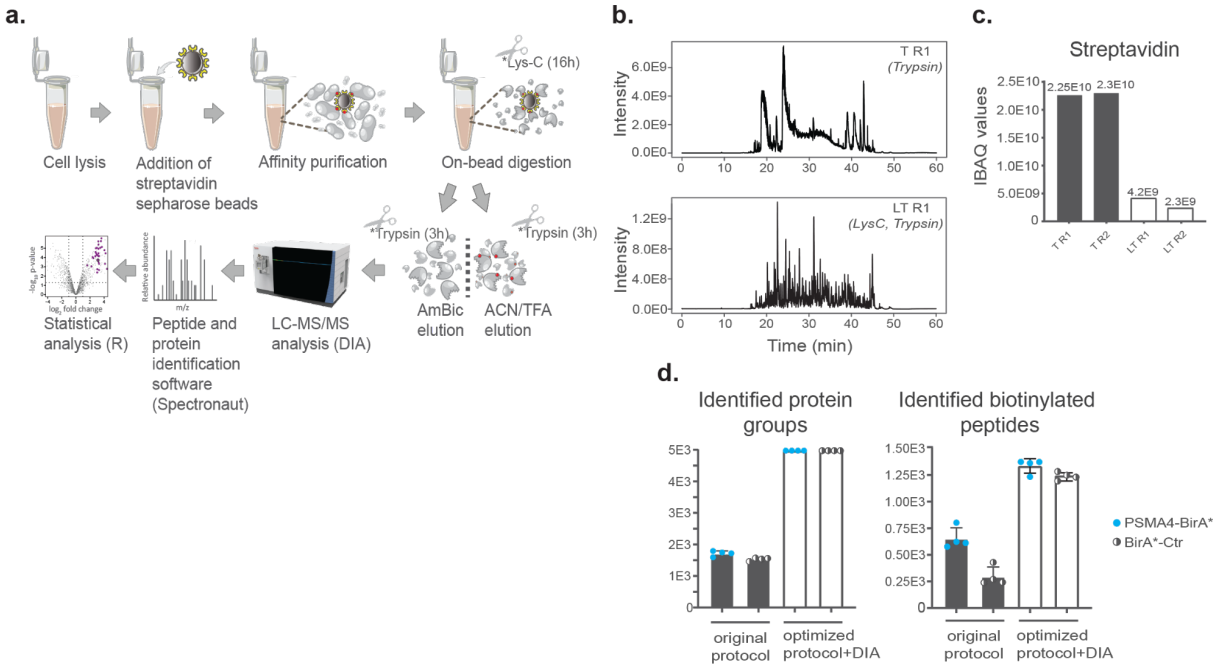

Supplemental figure 2: Optimization of BioID workflow

a. Scheme of optimized BioID protocol. The original protocol by Mackmull et al. [24] was optimized by (i) acetylation of lysines on streptavidin prior to pull-down; (ii) replacement of trypsin by LysC for on-bead digestion. Following on-bead digestion, two sequential elutions with ammonium bicarbonate (AmBic) and acetonitrile (ACN) / trifluoroacetic acid (TFA) are performed and eluates are further digested off-beads with trypsin. (iii) Peptides from AmBic and ACN/TFA eluates are then analyzed by Data Independent Acquisition (DIA) mass spectrometry.

b. Representative base peak chromatograms of AmBic elutions obtained from the original (upper panel,) and modified (lower panel) BioID protocol. The replacement of trypsin with LysC together with the acetylation of streptavidin drastically reduces the contamination by streptavidin-derived peptides.

c. Quantification of streptavidin in AmBic elutions obtained from the original (T: trypsin) and modified (LT: LysC followed by trypsin) BioID protocol. Streptavidin quantification was based on iBAQ values [49] obtained label free mass spectrometry analysis. Two representative replicates (R1, R2) are shown for each condition.

d. Barplots of the number of identified protein groups and biotinylated peptides obtained using the original vs. optimized BioID protocols. Data were obtained from cell lines expressing PSMA4-BirA* (light blue dots) or BirA* (black/white dots). The number of identified protein groups was obtained from AmBic samples, while the number of biotinylated peptides was derived from ACN/TFA samples. n = 4, biological replicates.

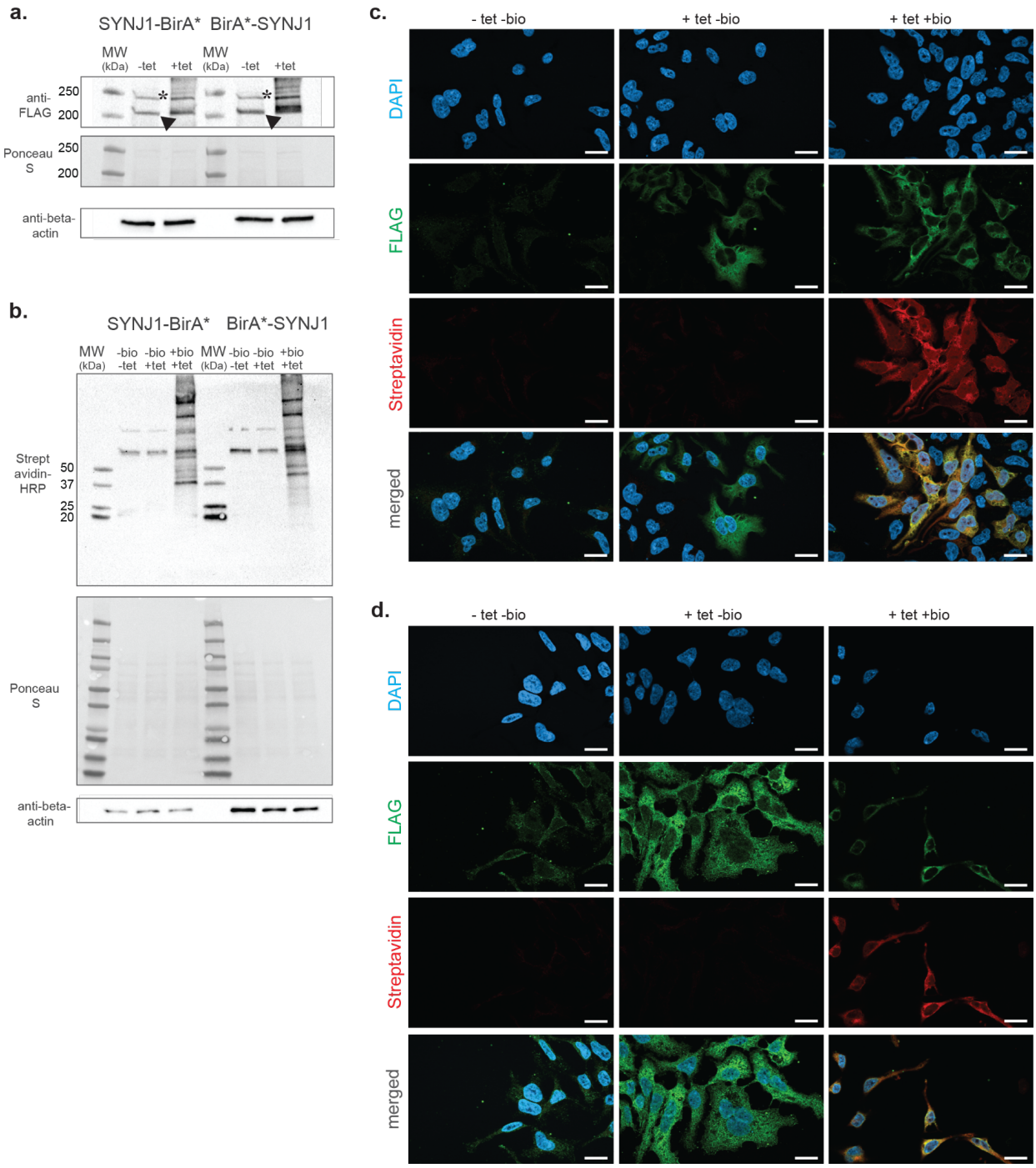

Supplemental figure 3: Validation of cell lines for SYNJ1 BioID

a. Immunoblot of BirA* fusion proteins performed on lysates collected from HEK293T cells stably transfected with SYNJ1-BirA*-FLAG or BirA*-FLAG-SYNJ1 following 24h incubation with (+tet) or without (−tet) tetracycline. Arrows indicate the protein band corresponding to

endogenous, untagged SYNJ1 protein, and stars indicate BirA* fusion proteins. Ponceau S staining and immunoblot against beta actin were used as loading controls.

b. Streptavidin-HRP blot following induction of BirA* fusion proteins with tetracycline and supplementation of biotin for 24h. Ponceau S staining and immunoblot against beta actin were used as loading controls. HRP: horseradish peroxidase.

c., d. Immunofluorescence analysis of SYNJ1-BirA*-FLAG (c.) and BirA*-FLAG-SYNJ1 (d.) cell lines 4 days after seeding without addition of any substance (-tet -bio), with addition of only tetracycline for 4 days (+tet -bio) or with addition of both tetracycline for 4 days and biotin for 1 day (+tet +bio). Scale bar indicates 20µm.

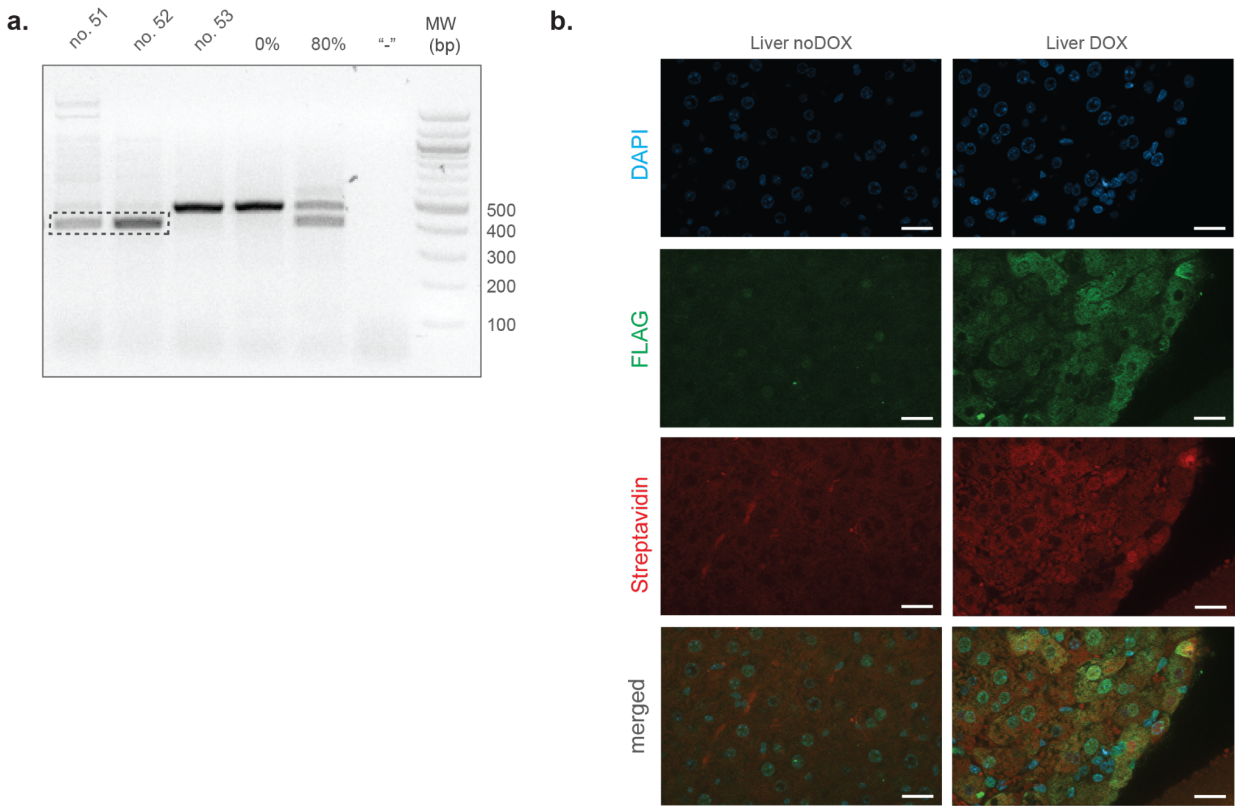

Supplemental figure 4: ProteasomeID mouse validation

a. Representative agarose gel illustrating successful excision of loxP-STOP-loxP (LSL) cassette by recombination at the CAGs-LSL-rtTA3 locus. Bands highlighted in the dotted square are PCR products amplified from the locus with an excised LSL cassette from two representative mice (no. 51 and no. 52). "0%" and "80%" samples represent control samples from mice showing no excision or approximately 80% excision of the LSL cassette, while "-" sample is a negative control with DNase free water added instead of the DNA template.

b. Immunofluorescence analysis of liver tissue from ProteasomeID mice fed with regular chow (left) or doxycycline containing food (right) for 14 days and submitted to 7 daily biotin injections. Scale bar indicates 20µm. DOX: mice fed with doxycycline containing food; noDOX - mice fed with regular chow.

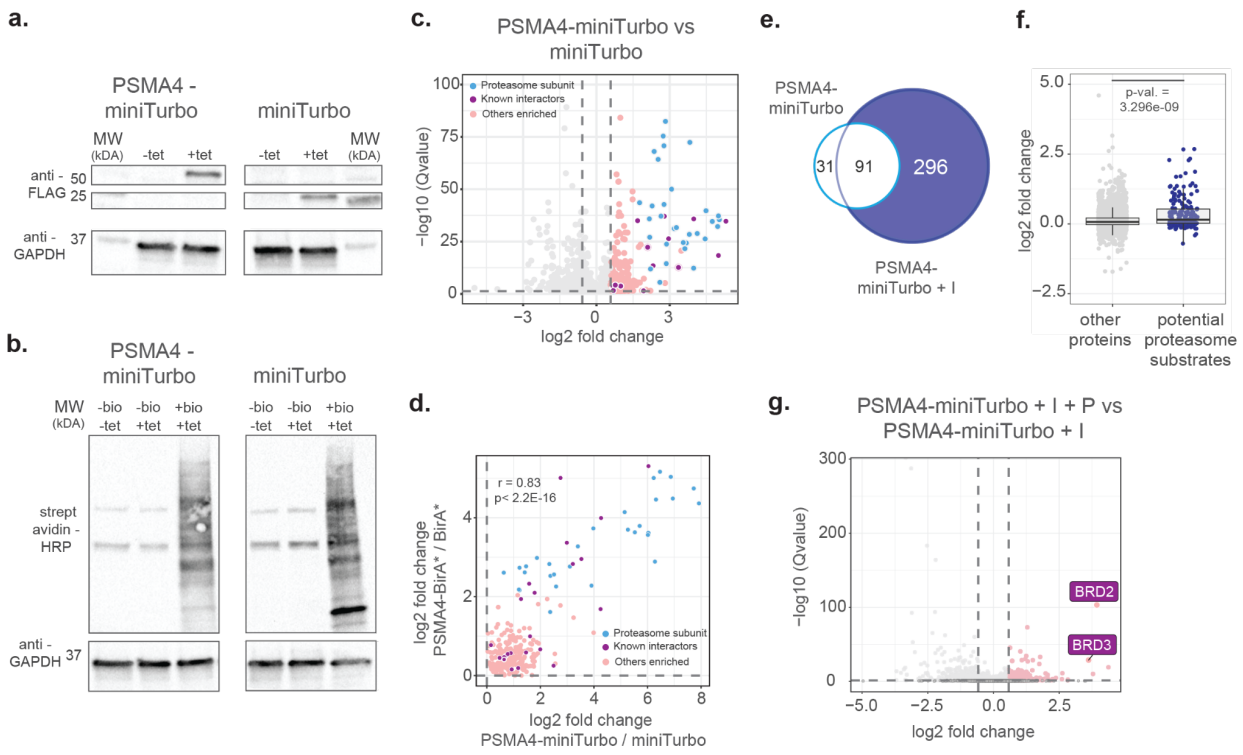

Supplemental figure 5: Validation of PSMA4-miniTurbo cell line and identification of potential proteasome substrates

a. Immunoblot of miniTurbo fusion proteins performed on lysates collected from HEK293T cells stably transfected with PSMA4-miniTurbo-FLAG or miniTurbo-FLAG following 4 days of incubation with (+tet) or without (−tet) tetracycline. Immunoblot against GAPDH was used as loading control.

b. Streptavidin-HRP blot following induction of miniTurbo fusion proteins with tetracycline and supplementation of biotin for 2 h. Immunoblot against GAPDH was used as loading control.

c. Volcano plot of proteins enriched by streptavidin pull-down and analyzed by DIA mass spectrometry from PSMA4-miniTurbo and miniTurbo control cell lines. Cut offs for enriched proteins: log2 fold change > 1 and Q value < 0.05. n = 4, biological replicates.

d. Comparison of log2 fold changes for streptavidin-enriched proteins from PSMA4-BirA* and PSMA4-miniTurbo compared to their respective controls. Proteins significant (Q value < 0.05) and displaying a log2 fold change > 0 in both comparisons were considered for the analysis.

e. Venn diagram showing the overlap between proteins significantly enriched in ProteasomeID samples (PSMA4-miniTurbo cells) with or without treatment with proteasome inhibitor MG132 (I). Proteins identified as significantly enriched only after MG132 treatment are considered as potential proteasome substrates. ProteasomeID data were filtered for log2 fold change > 1 and Q value < 0.05.

f. Comparison of log2 fold protein changes from the whole proteome analysis of HEK293T cells expressing PSMA4-miniTurbo upon MG132 treatment. Displayed log2 fold changes are averages of n = 4 biological replicates. P value was calculated using a Wilcoxon Rank Sum test with continuity correction. Potential proteasome substrates as defined in panel *e* are highlighted in blue.

g. Volcano plot of proteins enriched by streptavidin pull-down and analyzed by DIA mass spectrometry from PSMA4-miniTurbo cells treated with KB02-JQ1 PROTAC molecule (P) and PSMA4-miniTurbo cells treated with both PROTAC molecule (P) and MG132 proteasome inhibitor (I). Cut offs for enriched proteins: log2 fold change > 1 and Q value < 0.05. n = 4, biological replicates. Enrichment of BRD containing proteins is highlighted in violet boxes.

REFERENCES

1. Schmidt, M. & Finley, D. Regulation of proteasome activity in health and disease. *Biochim. Biophys. Acta* **1843**, 13–25 (2014).
2. Rousseau, A. & Bertolotti, A. Regulation of proteasome assembly and activity in health and disease. *Nat. Rev. Mol. Cell Biol.* **19**, 697–712 (2018).
3. Glickman, M. H. & Ciechanover, A. The ubiquitin-proteasome proteolytic pathway: destruction for the sake of construction. *Physiol. Rev.* **82**, 373–428 (2002).
4. Abildgaard, A. B. *et al.* Co-Chaperones in Targeting and Delivery of Misfolded Proteins to the 26S Proteasome. *Biomolecules* vol. 10 1141 (2020).
5. Saez, I. & Vilchez, D. The Mechanistic Links Between Proteasome Activity, Aging and Age-related Diseases. *Curr. Genomics* **15**, 38–51 (2014).
6. Tanaka, K. & Matsuda, N. Proteostasis and neurodegeneration: the roles of proteasomal degradation and autophagy. *Biochim. Biophys. Acta* **1843**, 197–204 (2014).
7. Vilchez, D. *et al.* RPN-6 determines C. elegans longevity under proteotoxic stress conditions. *Nature* **489**, 263–268 (2012).
8. Kelmer Sacramento, E. *et al.* Reduced proteasome activity in the aging brain results in ribosome stoichiometry loss and aggregation. *Mol. Syst. Biol.* **16**, e9596 (2020).
9. Tonoki, A. *et al.* Genetic evidence linking age-dependent attenuation of the 26S proteasome with the aging process. *Mol. Cell. Biol.* **29**, 1095–1106 (2009).
10. Nguyen, N. N. *et al.* Proteasome β5 subunit overexpression improves proteostasis during aging and extends lifespan in Drosophila melanogaster. *Sci. Rep.* **9**, 3170 (2019).
11. Chondrogianni, N. *et al.* Central role of the proteasome in senescence and survival of human fibroblasts: induction of a senescence-like phenotype upon its inhibition and resistance to stress upon its activation. *J. Biol. Chem.* **278**, 28026–28037 (2003).
12. Chondrogianni, N. & Gonos, E. S. Proteasome inhibition induces a senescence-like phenotype in primary human fibroblasts cultures. *Biogerontology* **5**, 55–61 (2004).
13. Manasanch, E. E. & Orlowski, R. Z. Proteasome inhibitors in cancer therapy. *Nature Reviews Clinical Oncology* vol. 14 417–433 (2017).
14. Feist, E., Burmester, G.-R. & Krüger, E. The proteasome — victim or culprit in autoimmunity. *Clinical Immunology* vol. 172 83–89 (2016).
15. Zeng, S. *et al.* Proteolysis targeting chimera (PROTAC) in drug discovery paradigm: Recent progress and future challenges. *Eur. J. Med. Chem.* **210**, 112981 (2021).
16. Pettersson, M. & Crews, C. M. PROteolysis TArgeting Chimeras (PROTACs) - Past, present and future. *Drug Discov. Today Technol.* **31**, 15–27 (2019).
17. Garber, K. The PROTAC gold rush. *Nat. Biotechnol.* **40**, 12–16 (2022).
18. Abi Habib, J., Lesenfants, J., Vigneron, N. & Van den Eynde, B. J. Functional Differences between Proteasome Subtypes. *Cells* **11**, (2022).
19. Marshall, R. S. & Vierstra, R. D. Dynamic Regulation of the 26S Proteasome: From

Synthesis to Degradation. *Front Mol Biosci* **6**, 40 (2019).
20. Albert, S. *et al.* Proteasomes tether to two distinct sites at the nuclear pore complex. *Proc. Natl. Acad. Sci. U. S. A.* **114**, 13726–13731 (2017).
21. Albert, S. *et al.* Direct visualization of degradation microcompartments at the ER membrane. *Proc. Natl. Acad. Sci. U. S. A.* **117**, 1069–1080 (2020).
22. Eisenberg-Lerner, A. *et al.* Golgi organization is regulated by proteasomal degradation. *Nat. Commun.* **11**, 409 (2020).
23. Ramachandran, K. V. & Margolis, S. S. A mammalian nervous-system-specific plasma membrane proteasome complex that modulates neuronal function. *Nat. Struct. Mol. Biol.* **24**, 419–430 (2017).
24. Mackmull, M.-T. *et al.* Landscape of nuclear transport receptor cargo specificity. *Mol. Syst. Biol.* **13**, 962 (2017).
25. Fabre, B. *et al.* Deciphering preferential interactions within supramolecular protein complexes: the proteasome case. *Mol. Syst. Biol.* **11**, 771 (2015).
26. Haffner, C. *et al.* Synaptojanin 1: localization on coated endocytic intermediates in nerve terminals and interaction of its 170 kDa isoform with Eps15. *FEBS Lett.* **419**, 175–180 (1997).
27. Mani, M. *et al.* The Dual Phosphatase Activity of Synaptojanin1 Is Required for Both Efficient Synaptic Vesicle Endocytosis and Reavailability at Nerve Terminals. *Neuron* vol. 56 1004–1018 (2007).
28. Drouet, V. & Lesage, S. Synaptojanin 1 mutation in Parkinson's disease brings further insight into the neuropathological mechanisms. *Biomed Res. Int.* **2014**, 289728 (2014).
29. Soda, K. *et al.* Role of dynamin, synaptojanin, and endophilin in podocyte foot processes. *J. Clin. Invest.* **122**, 4401–4411 (2012).
30. Fredriksson, S. *et al.* Protein detection using proximity-dependent DNA ligation assays. *Nat. Biotechnol.* **20**, 473–477 (2002).
31. Branon, T. C. *et al.* Efficient proximity labeling in living cells and organisms with TurboID. *Nat. Biotechnol.* **36**, 880–887 (2018).
32. Dow, L. E. *et al.* Conditional reverse tet-transactivator mouse strains for the efficient induction of TRE-regulated transgenes in mice. *PLoS One* **9**, e95236 (2014).
33. Nagy, A. Cre recombinase: the universal reagent for genome tailoring. *Genesis* **26**, 99–109 (2000).
34. Heink, S., Ludwig, D., Kloetzel, P.-M. & Krüger, E. IFN-gamma-induced immune adaptation of the proteasome system is an accelerated and transient response. *Proc. Natl. Acad. Sci. U. S. A.* **102**, 9241–9246 (2005).
35. Rechsteiner, M. & Hill, C. P. Mobilizing the proteolytic machine: cell biological roles of proteasome activators and inhibitors. *Trends Cell Biol.* **15**, 27–33 (2005).
36. Trulsson, F. *et al.* Deubiquitinating enzymes and the proteasome regulate preferential sets of ubiquitin substrates. *Nat. Commun.* **13**, 2736 (2022).

37. Zhang, X., Crowley, V. M., Wucherpfennig, T. G., Dix, M. M. & Cravatt, B. F. Electrophilic PROTACs that degrade nuclear proteins by engaging DCAF16. *Nat. Chem. Biol.* **15**, 737–746 (2019).
38. Koulich, E., Li, X. & DeMartino, G. N. Relative structural and functional roles of multiple deubiquitylating proteins associated with mammalian 26S proteasome. *Mol. Biol. Cell* **19**, 1072–1082 (2008).
39. Lee, H. Genetically Engineered Mouse Models for Drug Development and Preclinical Trials. *Biomolecules & Therapeutics* vol. 22 267–274 (2014).
40. Yim, C. W., Flynn, N. M. & Fitzgerald, F. T. Penetration of oral doxycycline into the cerebrospinal fluid of patients with latent or neurosyphilis. *Antimicrob. Agents Chemother.* **28**, 347–348 (1985).
41. Fornasiero, E. F. *et al.* Precisely measured protein lifetimes in the mouse brain reveal differences across tissues and subcellular fractions. *Nat. Commun.* **9**, 4230 (2018).
42. Guo, Q. *et al.* In Situ Structure of Neuronal C9orf72 Poly-GA Aggregates Reveals Proteasome Recruitment. *Cell* **172**, 696–705.e12 (2018).
43. Wolf-Levy, H. *et al.* Revealing the cellular degradome by mass spectrometry analysis of proteasome-cleaved peptides. *Nat. Biotechnol.* (2018) doi:10.1038/nbt.4279.
44. Storey, J. D. A direct approach to false discovery rates. *Journal of the Royal Statistical Society: Series B (Statistical Methodology)* vol. 64 479–498 (2002).
45. Perez-Riverol, Y. *et al.* The PRIDE database and related tools and resources in 2019: improving support for quantification data. *Nucleic Acids Res.* **47**, D442–D450 (2019).
46. Chen, S. *et al.* Structural basis for dynamic regulation of the human 26S proteasome. *Proc. Natl. Acad. Sci. U. S. A.* **113**, 12991–12996 (2016).
47. Pettersen, E. F. *et al.* UCSF Chimera?A visualization system for exploratory research and analysis. *Journal of Computational Chemistry* vol. 25 1605–1612 (2004).
48. Miyazaki, J. *et al.* Expression vector system based on the chicken beta-actin promoter directs efficient production of interleukin-5. *Gene* **79**, 269–277 (1989).
49. Cox, J. & Mann, M. MaxQuant enables high peptide identification rates, individualized p.p.b.-range mass accuracies and proteome-wide protein quantification. *Nature Biotechnology* vol. 26 1367–1372 (2008).